Department of Precision and Microsystems Engineering

Structural and Mass Optimization of Lunar Zebro Chassis with Carbon Fiber Reinforced Polymer

Prateek Garg

Report no : 2025.058
Coach : Dr.Ir. J.F.L. Goosen
Professor : Dr.Ir. J.F.L. Goosen
Specialisation : Computational Design and Mechanics
Type of report : Master Thesis
Date : 5 September 2025

Preface

This master's thesis presents research on the use of Carbon Fiber Reinforced Polymer (CFRP) for the structural and mass optimization of the Lunar Zebro chassis. The study was completed as part of the High-Tech Engineering program at the TU Delft Department of Precision and Microsystems Engineering in order to graduate.

My academic career has been significantly impacted by my keen interest in computational design and materials science. The engineering, analysis, and customization of cutting-edge materials for high-performance applications have always piqued my attention. This interest, together with my long-standing curiosity about the exploration of space and the technical challenges it brings, led me to pursue a thesis on the mechanical design of space-bound systems.

With its goal of enabling robust and compact lunar mobility, the Lunar Zebro project offered the perfect setting for me to pursue my passion. I was able to contribute to a practical application that might one day be used on the Moon while delving deeply into the mechanics of composite structures, simulation-driven design, and failure analysis in harsh environments.

I want to sincerely thank Dr. Ir. J.F.L. Goosen for his constant guidance, constructive feedback, and unwavering support during this study. His advice greatly influenced the approach and course of this thesis.

Lastly, I want to express my gratitude to my family and everyone else who supported me during this academic journey.

August 2025,
Prateek Garg

Abstract

One of the main challenges in designing space-bound robotic platforms, like the Lunar Zebro, a six-legged nano rover meant for deployment on the Moon, is creating a lightweight and structurally efficient chassis. With an emphasis on minimizing mass and maintaining structural integrity under launch-induced loads, this study investigates the use of Carbon Fiber Reinforced Polymer (CFRP) as an alternative to conventional materials like Aluminium for the chassis. The Solid Mechanics and Layered Shell module of COMSOL Multiphysics was used to perform simulations to examine and contrast the mechanical responses of the two materials.

The study builds on this basis by simulating launch acceleration through plate modelling with a 10g body load. While CFRP plates are evaluated using Tsai-Wu failure analysis and cohesive zone modelling to monitor delamination risks, Aluminium plates of different thicknesses are evaluated for stress response using von Mises criteria. With all plies staying within safe limits in CFRP, this comparative analysis reveals that CFRP at 1 mm thickness shows less displacement than even a 2 mm thick Aluminium plate. These results direct the investigation's subsequent phase, which involves optimizing the thickness and ply orientation. To find the ideal balance between stiffness, displacement, and failure safety, several layup configurations are simulated, including [0/90/90/0], [0/45/-45/0], and [0/90/0/90/0]. The ideal laminate is a cross-ply arrangement with a thickness of 0.69 mm, which can reduce material mass by roughly 72% while matching the stiffness of 1.5 mm Aluminium.

After that, the study switches from flat plates to a complete 3D chassis model, which depicts the rover's structural enclosure. Six CFRP plates make up a simplified box structure examined in static and dynamic settings. To possible mounting configurations on a lunar lander, several box orientations and constraint sizes are tested. To guarantee vibrational safety, eigenfrequency analysis is performed, and constraint refinement allows first mode frequencies to surpass 100 Hz. In addition, geometric changes are investigated, first by switching from a cuboidal to a lofted and tapered chassis profile. Each is assessed for mass, internal volume, displacement performance, and dynamic response. In comparison to the baseline cuboid geometry, the mass was further decreased by 7.44% after reducing the mass by 72% through material change (implementation of CFRP instead of Aluminium) while the stiffness was raised in case of lofted geometry.

Internal rib reinforcements and external geometric stiffeners modelled based on sheet metal forming and plastic extrusion are added to further improve structural efficiency. One notable improvement among these is a lofted ribbed configuration with two internal ribs and thinner walls. Compared to the original cuboid reference geometry, this combination maintained low displacement, ensured dynamic safety with a first eigenfrequency close to 195 Hz, and reduced overall mass by 40.7%. When the rectangular cell geometric feature was added to the chassis side walls, displacement decreased by 8.5% while mass increased by only 1.2%. Because there was room for it, the stiffness increased with the least amount of mass penalty. An organized design process for lightweight, high-performance rover chassis made of CFRP is provided by the integrated approach, which extends from fundamental material modelling to system-level geometric and structural optimization. The study offers a thorough framework for structurally optimizing small-scale lunar vehicles through the layered evaluation of materials, shapes, and reinforcements.

Table of Contents

1. Introduction 1
1.1. Background 1
1.1.1. Material Selection 1
1.1.1.1. Properties of CFRP 2
1.1.2. Chassis Design 3
1.1.2.1. Chassis Design Concepts (Automotive chassis) 4
1.2. State of the Art 4
1.2.1. Rover chassis evolution 4
1.2.2. Design features 6
1.2.3. Use of Finite Element Analysis 7
1.3. Problem Statement 8
2. Research Approach 10
2.1. Motivation 10
2.2. Objective 10
2.3. Proposal 10
2.4. Methodology 11
3. Chassis Surface Modelling 12
3.1. Stress Analysis of Aluminium Plate under Body Load 12
3.2. Failure criteria check for CFRP 13
3.2.1. Delamination Analysis using Cohesive Zone Modelling 13
3.2.2. Tsai-Wu Failure Analysis (Ply-Level Integrity) 14
3.3. Comparative analysis based on displacement and mass 16
3.4. Optimization Strategy for Ply Design 18
3.4.1. Ply Orientation Modelling 19
3.4.2. Thickness Optimization Following Ply Orientation 20
4. Chassis Box Modelling and Material Comparison 23
4.1. Simulation Setup and Workflow 23
4.2. Stress Response and Safety Margin 25
4.3. Displacement Analysis 25
4.4. Ply Orientation Sensitivity in Thin-Walled Box 26
4.5. Effect of Global Box Orientation with Respect to Body Load 27
4.6. Modal Performance and Constraint-Size Optimization 28
4.7. Consolidated Design Definition 28
5. Design 30
5.1. Shape Modification 30

5.1.1. Lofted Geometry: Conceptual and Mechanical Evaluation 30
5.1.1.1. Mass Comparison and Structural Response 31
5.1.1.2. Modal Performance and Center of gravity (CoG) 32
5.1.1.3. Analytical calculations of CoG 32
5.1.2. Taper Geometry: Conceptual and Mechanical Evaluation 32
5.1.2.1. Mass Comparison and Structural Response 33
5.1.2.2. Modal Performance 33
5.1.3. Comparative analysis between Cuboid, Tapered and Lofted Geometry 34
5.2. Reinforcements 35
5.2.1. Static Analysis 36
5.2.2. Dynamic Analysis 36
5.2.3. Comparison flow based on Eigenfrequency, Displacement and Mass 37
5.2.4. Tsai-Wu Criterion to Validate Failure Index 38
5.2.5. Reduction of wall thickness of Lofted ribbed geometry 39
5.2.6. Orientation of the Lofted ribbed geometry 39
5.3. Geometric Stiffeners 41
5.3.1. Geometric Stiffener Concepts 42
5.3.2. Implementation of Rectangular cell feature 43
5.3.3. Comparative analysis between different stiffening features 45
5.3.4. The Final design of the Chassis 46
6. Conclusion 47
7. Recommendations for Future Work 49
8. Appendix 50
Bibliography 54

List of Figures

Figure 1: Lunar Zebro 1
Figure 2: Relative importance of metals, polymers, composites, and ceramics as a function of time. The diagram is schematic and describes neither tonnage nor value. The timescale is nonlinear. 2
Figure 3: CFRP Sheets 2
Figure 4: Various types of chassis 4
Figure 5: Apollo Lunar Rover 5
Figure 6: Sojourner Rover 5
Figure 7: Spirit and Opportunity Rovers 5
Figure 8: Perseverance Rover 5
Figure 9: ExoMars Rover 6
Figure 10: Geometries of the different cross-sectioned stiffeners: (a) Type I (semicircular), (b) Type II (rectangular), and (c) Type III (trapeziform). 6
Figure 11: Hoffman safety factors at ply midplanes for the laminated composite shell 7
Figure 12: Geometric Model of all beams of the chassis in NX Software 8
Figure 13: Results of the meshing finite element: (a) Element Quality of mesh; (b) Image of mesh on the beams 8
Figure 14: Boundary conditions showing fixed constraint (left) and body load (right) 12
Figure 15: Von Mises stress distribution in Aluminium plates under 10g body load for thicknesses of 2 mm, 1.5 mm, and 1 mm (left to right). 12
Figure 16: Laminate structure and material input table for 1 mm CFRP with five 0° plies 13
Figure 17: Mode I and Mode II of the Delamination as modelled in CZM 14
Figure 18: Damage plot showing no delamination (damage = 0 across all interfaces) 14
Figure 19: Tsai-Wu surface plot for CFRP plate showing safe stress regions below failure limit. 16
Figure 20: Displacement plot of Aluminium plates of varying thicknesses 17
Figure 21: Displacement plot of CFRP plates of varying thicknesses 17
Figure 22: Optimization flow 18
Figure 23. Displacement vs. Thickness Plotfor Cross-Ply CFRP Laminates for locating the thickness at Aluminium displacement benchmark (0.13549) through intersection of this target vale with the displacement curve 22
Figure 24: Boundary conditions showing fixed constraint (left) and body load (right) 23
Figure 25: Workflow of developing and analyzing box chassis 24
Figure 26: Von Mises stress distribution in box under 10g body load for CFRP (left) and Aluminium (right) 25
Figure 27: Displacement plot of CFRP and Aluminium 25
Figure 28. View of Bottom wall 26
Figure 29: Stress plot and Displacement Magnitude plot of Orientation 2 (top) and Orientation 3 (bottom) of the cuboid chassis 27
Figure 30: Displacement (left) and stress response (right) of the optimized CFRP chassis under 10g body load (Z-direction) 29
Figure 31: Lofted geometry in COMSOL 31
Figure 32: Displacement and stress distribution of Lofted geometry 31
Figure 33: Tapered geometry in COMSOL 33
Figure 34: Displacement and stress distribution of Tapered geometry 33
Figure 35: Rib Stiffener 35
Figure 36: Static Analysis of cuboid with ribs 36
Figure 37: Tapered and Lofted geometries with ribs 36
Figure 38: Displacement plot of Lofted geometry with 2 ribs with wall and rib thickness being 0.435 mm 39
Figure 39. Stress plot and Displacement Magnitude plot of Orientation 2 of the Lofted chassis 40
Figure 40: Stress plot and Displacement magnitude plot of Orientation 3 of the Lofted chassis 40
Figure 41: Sheet metal design, Vacuum formed products and Aeroplane Wing panel depicting the geometric features 41
Figure 42: Different geometric features made in AutoCAD 43
Figure 43: Dimensions of the Dimple features (All dimensions are in mm) 43
Figure 44: Stress distribution and displacement plot for the lofted geometry with ribs integrating rectangular cell feature 44
Figure 45: Different geometric features for stiffening in COMSOL 45

FIGURE 46: FINAL CHASSIS DESIGN INCORPORATING CFRP MATERIAL, LOFTED GEOMETRY, RIBS AND RECTANGULAR CELL FEATURES 46

List of Tables

TABLE 1. PROPERTIES OF VARIOUS CARBON FIBER CLASSES 3
TABLE 2. MAXIMUM VON MISES STRESS AND INTERPRETATION FOR DIFFERENT ALUMINIUM PLATE THICKNESSES 13
TABLE 3. DAMAGE VARIABLE UNDER DELAMINATION 14
TABLE 4. TSAI-WU INDEX 15
TABLE 5. TSAI-WU INDEX OF CFRP PLATE 16
TABLE 6. CFRP AND ALUMINIUM AT VARIOUS THICKNESSES 17
TABLE 7. MATERIAL COMPARISON BASED ON MASS, DISPLACEMENT, AND FAILURE MODES 18
TABLE 8. TYPICAL TYPES OF ORIENTATIONS AND THEIR LAMINATE SEQUENCES OF STACKING 19
TABLE 9. DISPLACEMENT COMPARISON FOR DIFFERENT LAYUPS AT 1 MM THICKNESS 19
TABLE 10. EFFECT OF NUMBER OF LAYERS IN CROSS-PLY LAYUPS (TOTAL THICKNESS = 1 MM) 20
TABLE 11. THICKNESS OPTIMIZATION RESULTS FOR CFRP CROSS-PLY LAMINATES 21
TABLE 12. LAYER ORIENTATION VS DISPLACEMENT IN FULL CFRP BOX 26
TABLE 13. FIRST SIX MODAL FREQUENCIES OF THE CFRP BOX WITH 68 MM × 68 MM SQUARE CONSTRAINT 28
TABLE 14. EIGENFREQUENCIES OF LOFTED GEOMETRY 32
TABLE 15. EIGENFREQUENCIES OF TAPERED GEOMETRY 34
TABLE 16. MODAL, DISPLACEMENT, AND MASS DIFFERENCES BETWEEN THE THREE GEOMETRIES 34
TABLE 17. INTERNAL VOLUME COMPARISON BETWEEN THE THREE GEOMETRIES 34
TABLE 18. EIGENFREQUENCIES OF CUBOID WITH RIBS 36
TABLE 19. COMPARISON FLOW OF ALL RIBBED GEOMETRIES 37
TABLE 20. TSAI-WU INDEX OF THE DIFFERENT CONFIGURATIONS 38
TABLE 21. WALL THICKNESS REDUCTION AND EVALUATION OF DISPLACEMENT, MASS AND EIGENFREQUENCY 39
TABLE 22. DISPLACEMENT OF LOFTED RIBBED GEOMETRY COMPARED TO CUBOID IN DIFFERENT CHASSIS ORIENTATIONS 40
TABLE 23. COMPARATIVE ANALYSIS BETWEEN THE LOFTED RIBBED CONFIGURATION WITHOUT FEATURE VS WITH RECTANGULAR CELL FEATURE 44
TABLE 24. COMPARATIVE ANALYSIS OF DIFFERENT FEATURES BASED ON EIGENFREQUENCY, DISPLACEMENT AND MASS 45

List of Abbreviations

CFRP	Carbon Fiber Reinforced Polymer
FEA	Finite Element Analysis
CAD	Computer Aided Design
CAM	Computer Aided Manufacturing
LRV	Lunar Roving Vehicle
FEM	Finite Element Method
CZM	Cohesive Zone Modelling
CoG	Center of Gravity

1. Introduction

1.1. Background

The Lunar Zebro is a six-legged nano rover developed with the goal of enabling, lightweight and low-cost surface exploration of the Moon. This rover, which aims to be the smallest and lightest of its kind, makes use of minimalism and simplicity in both form and function. In contrast to traditional wheeled systems, Lunar Zebro's C-shaped legs enable it to move over uneven ground while preserving mechanical redundancy and robustness. Its structure must endure the harsh lunar environment, which is marked by vacuum, micrometeorite impacts, and sharp temperature gradients, as well as the tremendous launch accelerations and space travel vibrations.

Although it has a distinct mechanical identity due to its leg-based locomotion, the central chassis is still an essential part that must support structural loads during launch and deployment in addition to housing electronics, power systems, and payloads. The Zebro's early design iterations placed a strong emphasis on modularity and ease of manufacturing with conventional materials like Aluminium. However, the need for additional mass optimization and structural strengthening has become critical as the drive for efficiency and miniaturization intensifies.

A more thorough examination of the materials utilized as well as the design and construction of the structure is necessary to achieve this balance. Therefore, the emphasis switches to how meticulous design and material qualities can work together to produce a frame that is stronger, lighter, and more equipped to withstand the trip from Earth to the Moon and function well once there. According to this thesis, the first step in accomplishing this objective is to examine earlier studies and technological advancements to pinpoint tactics that promote this balance between light weight and maximum resilience. To guide the design and development of an optimized rover chassis, important insights are obtained from this background and state-of-the-art review.

Figure 1: Lunar Zebro

1.1.1. Material Selection

Strong launch loads, challenging lunar terrain, and large temperature gradients are all encountered by lunar rovers. Aluminium alloys have historically been favoured for chassis because of their strength and manufacturing ability. However, their high density is a major issue for planetary missions that restricts mass optimization. Because composite materials can combine high mechanical strength with reduced weight, they have become a promising alternative in recent decades. Metals, polymers, ceramics, and composites are the four fundamental categories into which structural materials can be separated. _[1] Typically,

different combinations of the other three materials are used to create composites, which are structural units made up of two or more separate materials. Figure 2 schematically illustrates the steadily growing significance of polymers, composites, and ceramics, and the diminishing role of metals. The paper [2] presents the relative importance of the four basic materials in a historical context. Because they have desirable qualities that none of the component materials alone could achieve, composites are frequently used. The properties of composites, which are engineered materials created by embedding stiff, strong fibers into a lightweight matrix, can be customized for particular loading scenarios. Since many materials are much stronger and stiffer in fiber form than in bulk, fibrous reinforcement works incredibly well. Of these, Carbon Fiber Reinforced Polymer (CFRP) is notable for its remarkable strength-to-weight ratio and anisotropic characteristics, which allow for the customization of stiffness through fiber orientation. Although it is extensively utilized in aerospace, little is known about its systematic application to small-scale lunar rover chassis.

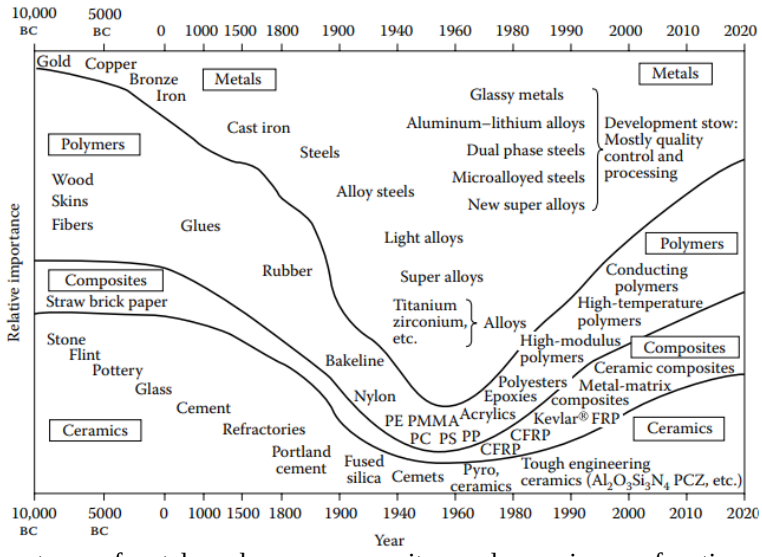

Figure 2: Relative importance of metals, polymers, composites, and ceramics as a function of time. The diagram is schematic and describes neither tonnage nor value. The timescale is nonlinear. [2]

1.1.1.1. Properties of CFRP

Figure 3: CFRP Sheets

Among modern engineering materials, CFRP stands out due to its remarkable fatigue and corrosion resistance, tunable anisotropy, and remarkable strength-to-weight ratio. It is especially well-suited for thin-walled chassis structures that will be subjected to the directional body loads and vibrations that are typical of a lunar rover during launch and surface navigation.

The density of CFRP is 1600 kg/m^3 which is very low and good for lightweight applications. Table 1 provides properties of CFRP material.

Fiber type	Acronym	Tensile strength [Gpa]	Young's modulus [Gpa]	Maximum elongation (%)
High tension	HT	3–5	200–250	1–2
Intermediate modulus	IM	4–7	250–350	1–2
High modulus	HM	2–4.5	350–450	<1
Ultra high modulus	UHM	~3	>700	<0.5

Table 1. Properties of various carbon fiber classes

The high modulus and specific tensile strength determined by the superiority of the graphite crystallites are among the primary characteristics. Carbon fibers are chosen to reduce the product's weight and replace traditional materials because of these characteristics. By increasing the crystal size and aligning them along the fiber axis, technological advancements resulted in an improved elastic modulus. [3]

Commercial carbon fibers have a high Young's modulus (between 200 and 500 GPa) and a high tensile strength (between 3 and 7 GPa). Additionally, carbon fibers have acceptable thermal and electrical conductivities. Their increased fatigue resistance is one of the main advantages of using these fibers in composite materials. Like glass or aramid fibers, carbon fibers do not experience stress rupture. [4]

The adoption of CFRP in automotive chassis, notably by manufacturers like BMW (i3, i8) and McLaren, demonstrates its potential for reducing mass while maintaining structural integrity. The use of sandwich panels, multi-material hybrid chassis, and topology-optimized designs has become a common practice to push performance boundaries. As electric and planetary vehicles (like lunar rovers) gain traction, similar design philosophies are being explored in lightweight, high-stiffness chassis structures.

1.1.2. Chassis Design

The vehicle's chassis is considered as its central frame, supporting all the loads and carrying all the components. These loads consist of the weight of every part as well as the forces generated during acceleration and deceleration. To absorb shock, twist, vibration, and other stresses, the chassis should be sufficiently rigid. In addition to strength for improved handling characteristics, resistance to bending and torsional stiffness are crucial factors in chassis design. [5] The chassis is often called the vehicle's backbone, as it determines its structure. The various functions of chassis are:

- The chassis ensures the vehicle's structural rigidity.
- It distributes the weight of all the components.
- Chassis materials need to possess high strength.
- Helps maintain the shape and prevents deformation.
- It plays a vital role in vehicle safety.

- Chassis design impacts vehicle stability and handling.
- Different types of chassis suit various vehicle applications. [6]

1.1.2.1. Chassis Design Concepts (Automotive chassis)

The chassis provides the foundation for the components of the vehicle with several designs which includes monocoque, ladder frame, tubular, and backbone chassis, see figure 4. Each design has unique advantages and disadvantages with regard to weight, performance and structural integrity. Like, the tubular chassis are ideal in competing for their strength-to-weight ratio while monocoque design incorporates the frame and body for enhanced rigidity and safety. [6]

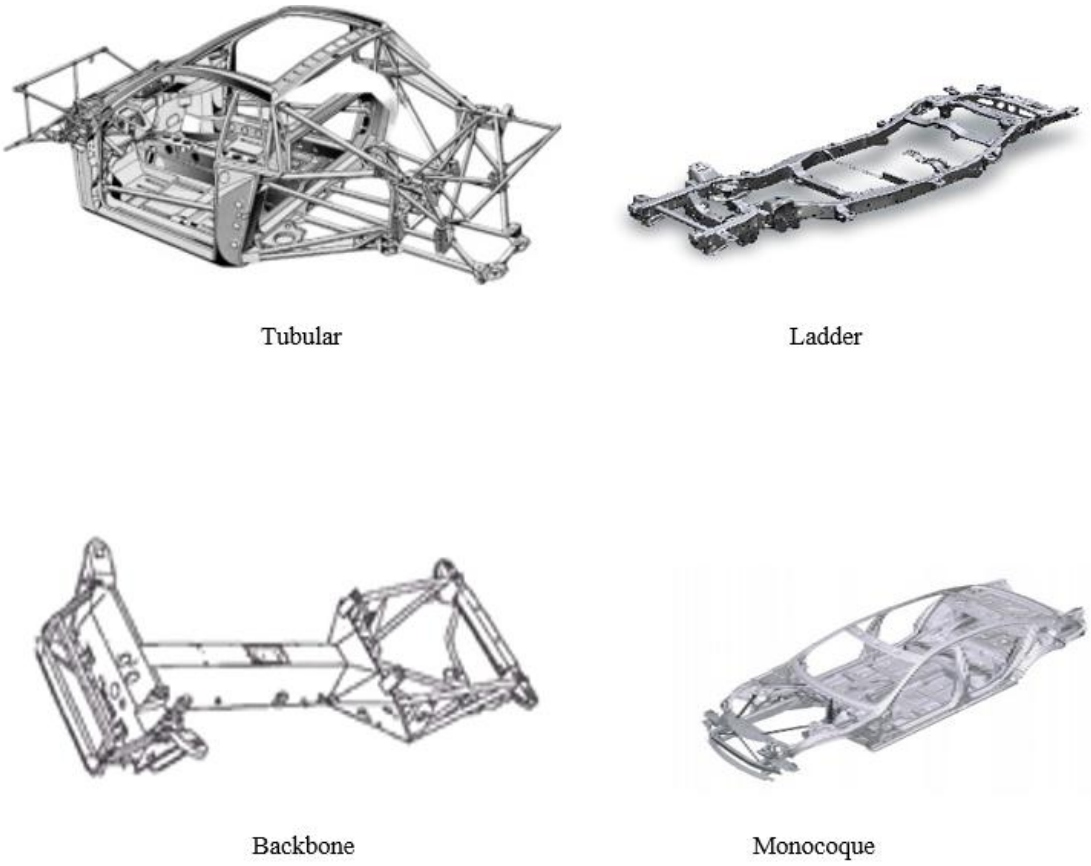

Figure 4: Various types of chassis

1.2. State of the Art

1.2.1. Rover chassis evolution

1. Apollo Lunar Rover (LRV):

The tubular chassis, a space frame made of welded Aluminium alloy tubes, was a feature of the Apollo Lunar Roving Vehicle (LRV). This method provided a sturdy yet lightweight framework that could be folded up for storage during launch. Though it lacked the material

efficiency and optimization found in modern designs, the tubular geometry offered distributed load paths and adequate resilience for the Moon's moderate gravity and rocky terrain. [7]

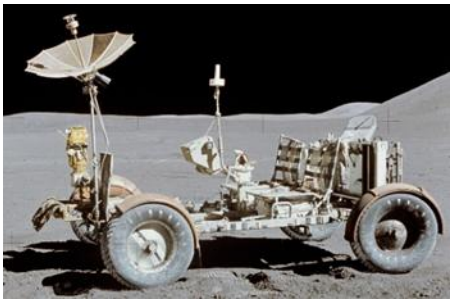

Figure 5: Apollo Lunar Rover

2. Sojourner (Mars Pathfinder):

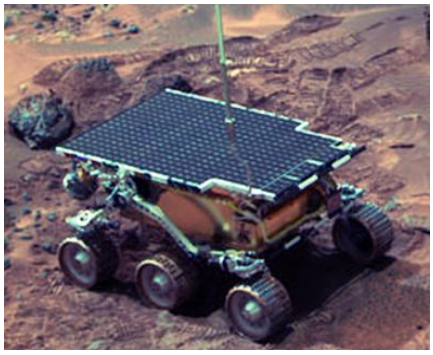

Figure 6: Sojourner Rover

A box-like chassis design was first used on the Martian surface by the Sojourner rover, which was a component of the Mars Pathfinder mission in the 1990s. Because of the careful engineering margins of the time, its structure was stiff and compact, but it was mainly made of stainless steel and Aluminium. The Sojourner's shape prioritized durability over mass savings, with little use of CAD tools or structural optimization. [8]

3. Spirit and Opportunity Rovers (Mars Exploration Rovers):

The arrival of Spirit and Opportunity, the Mars Exploration Rovers, marked a dramatic change. These rovers were more sophisticated, with better shock-absorbing suspension systems and better material distribution, but they still used box chassis shapes. The frames demonstrated a greater comprehension of load paths and center-of-gravity considerations, despite still being made of traditional metals. Now, these rovers could sustain larger payloads while remaining stable on the rough terrain of Mars. [9]

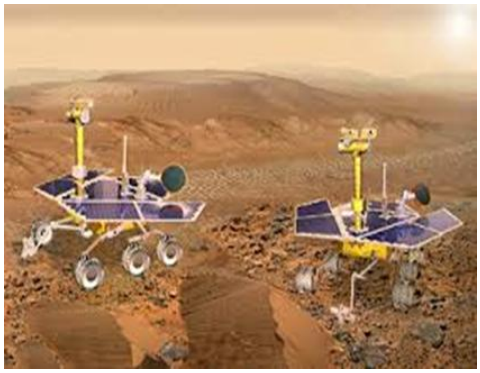

Figure 7: Spirit and Opportunity Rovers

4. Perseverance Rover (Mars 2020):

Figure 8: Perseverance Rover

The Perseverance rover was the pinnacle of planetary rover chassis design when it was launched in 2020 as a component of the Mars 2020 mission. The chassis in this instance was monocoque, combining the body and frame into a single load-bearing shell. As a result, NASA engineers were able to shape the external surfaces as structural elements and do away with superfluous internal framing. To arrive at forms that were both structurally robust and mass-efficient, the rover used topology optimization and finite element analysis (FEA). To preserve stiffness while lowering material volume, honeycomb sandwich panels were also added in strategic locations. [10]

***5. ExoMars Rover**:*

Similarly, Rosalind Franklin's ExoMars rover operated on a similar principle. The chassis was shaped using optimization algorithms to strategically thin out low-stress areas while reinforcing high-stress paths using a combination of titanium alloys and carbon fiber-reinforced polymers (CFRP). As a result, the structure's shapes frequently departed from strictly rectangular shapes and became lighter, more symmetrical, and better able to maintain payload balance. In recent decades, it was impossible to manufacture these non-uniform shapes, but due to advancements in CAD-CAM and additive manufacturing, they are now not only feasible but also preferred. [9]

Figure 9: ExoMars Rover

1.2.2. Design features

Geometrically embedded stiffening features have long been a tried-and-true way to improve mechanical performance in high-performance engineering structures, especially in the automotive and aerospace industries, without requiring appreciable mass increases. To prevent deformation under bending, shearing, or compressive loads, thin-walled panels are equipped with raised contours, hollow extrusions, or channel-like profiles.

Traditionally, additional thickness or material layering was used to achieve structural reinforcement. Nonetheless, form-driven stiffness is given priority in contemporary design methodologies, where geometry alone greatly influences mechanical behaviour. Common approaches include Ribs (Longitudinal or transverse features to resist bending and improve torsional rigidity), embosses, beads, etc. [11] [12]

Certain stiffening contours have been shown in numerous studies to increase structural efficiency. [13] Study examined the impact of various stiffening shapes on long glass fiber-reinforced polypropylene panels by contrasting semicircular, rectangular, and trapezoidal shapes. The findings demonstrated that rectangular shapes offered more resistance to overall displacement, while semicircular features offered superior buckling resistance. Conversely, trapezoidal contours provided competitive performance with more design flexibility by striking a balance between stiffness and manufacturability.

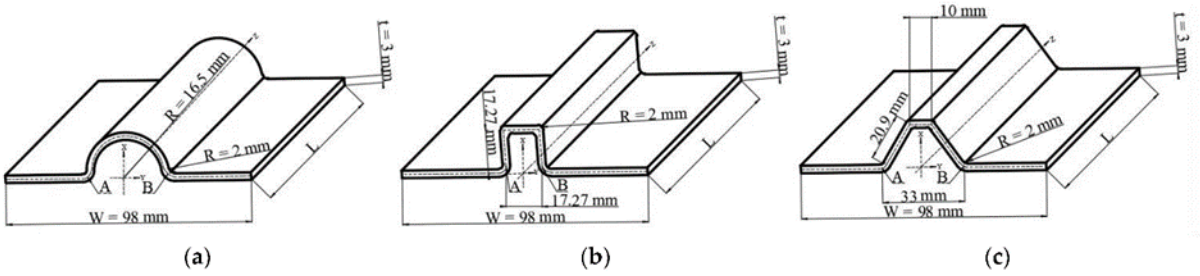

Figure 10: Geometries of the different cross-sectioned stiffeners: (**a**) Type I (semicircular), (**b**) Type II (rectangular), and (**c**) Type III (trapeziform).

Although these geometries have historically been used in cargo floors, car interiors, and electronic equipment enclosures, their underlying mechanical principles are not necessarily specific to those applications. Thin-walled chassis structures, where high strength-to-weight performance is crucial, can benefit from the same shape-dependent stiffness enhancement. In

these situations, adding non-flat surface profiles can improve stiffness locally or directionally, which lowers deflection and delays the onset of instability.

This method's potential integration with composite materials makes it particularly promising for use in the future. Such stiffening features can be directly incorporated into curved or flat panels during layup or molding processes because advanced fabrication techniques enable complex surface shaping even in materials like CFRP. In situations where stiffness is naturally achieved through shape, strategically placed geometric features can further improve structural integrity without relying only on laminate orientation or thickness changes. This allows for minimal mass penalty.

1.2.3. Use of Finite Element Analysis

There are numerous studies available which show the use of FEA to model CFRP and perform different mechanical analysis and present procedure adopted in these studies for particular applications. Due to its layered composite structure, CFRP shows anisotropic behaviour. This requires specialized and focused finite element modelling approach. This approach should be able to capture ply orientations, failure mechanisms, and stacking sequence. [14]

One study utilized a layered composite shell model with a [90/−45/45/0] stacking sequence, capturing the anisotropic elastic properties of each ply. It also highlights that COMSOL's layered shell modelling and integrated failure criteria are robust tools for validating CFRP structural designs, especially when evaluating mechanical load integrity in chassis-like thin-walled components. [15]

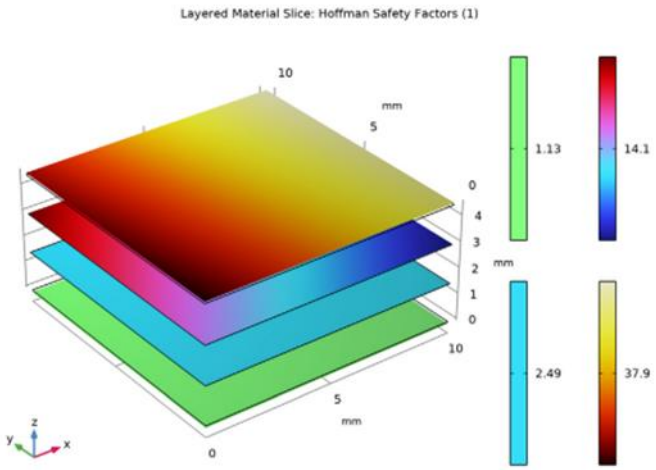

Figure 11: Hoffman safety factors at ply midplanes for the laminated composite shell

Another study where analysis of the vibration characteristics of chassis was based on the numerical method and the FE model of the chassis was required and validated by the measured results obtained throughout the production. The FE model used was Ansys Workbench software for the analysis of the forced vibration of the chassis to predict the excitation at the hung-mass. For the FE model of the chassis, firstly, a geometrical model was required. The geometrical model for the components of the 29-seat bus chassis was used for this research. [16]

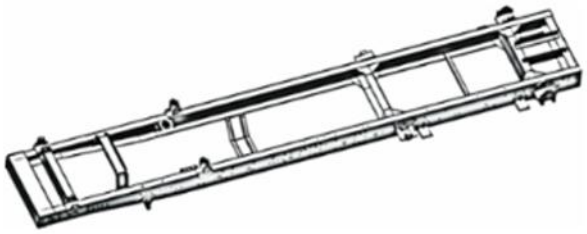

Figure 12: Geometric Model of all beams of the chassis in NX Software

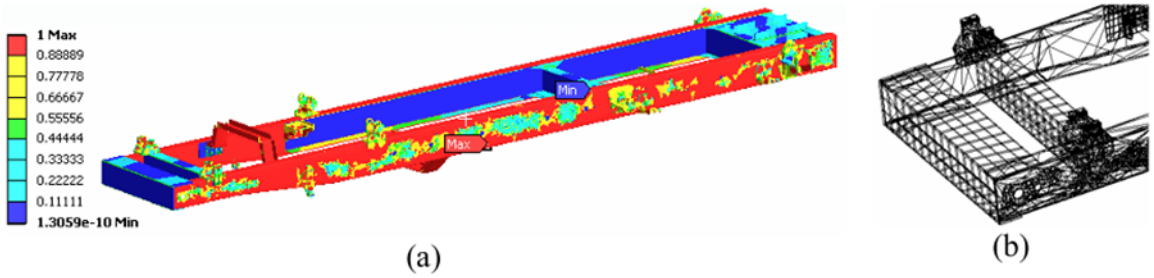

Figure 13: Results of the meshing finite element: (a) Element Quality of mesh; (b) Image of mesh on the beams

The FEA methodology present in the studies provides a foundation and is essential for optimizing the Lunar Zebro chassis as well by accurately predicting stress distributions, vibrations, and deformations under lunar conditions and simulating load cases (static and dynamic) to identify potential design weaknesses. It would also help to validate material performance under extreme lunar environmental conditions and mechanical stresses.

The review of existing rover design and material technologies reveals a clear evolution toward structurally efficient systems that leverage both material capabilities and geometric refinement to meet mission-specific demands. From the monocoque shells of advanced Martian rovers to the strategic material tailoring observed in more recent designs, it becomes evident that structural optimization is no longer a matter of strength alone, but of achieving performance through precise trade-offs between mass, stiffness, and manufacturability.

1.3. Problem Statement

Literature predominantly focuses on its use in large, wheeled rovers. For legged micro-rovers like the Lunar Zebro, systematic investigations on how CFRP can be adapted for thin-walled, compact structures subjected to unique body-loading scenarios (e.g., mounting loads and point excitations) are sparse. The ways in which ply orientation, thickness, and composite layup can be adjusted for such scale and loading circumstances have not been thoroughly investigated.

To minimize weight and effectively distribute loads, modern rovers are increasingly depending on monocoque or hybrid chassis designs. However, most existing research either focuses on wheeled rovers or large rovers using bulk Aluminium designs. A literature gap exists in adapting monocoque design principles for highly compact, leg-based locomotion systems with constraints on mass, internal volume, and localized impact loading (such as at leg mounting points). Furthermore, the link between shape, material choice, and mass distribution for such compact systems remains underexplored.

Numerous studies highlight the mechanical benefits of embedded stiffening features, semi-circular contours, ribs, rectangular reinforcements in sheet metals, and automotive enclosures.

While promising, their transfer to space-grade composite chassis remains theoretical, especially in micro-rover platforms. The practical implementation of geometric stiffeners in CFRP and their effect on displacement and eigenfrequencies has not yet been investigated in the context of rovers. There is a research opportunity to understand how such features affect the localized deformation around legs and external loads without compromising manufacturability or internal housing space.

The **research question** therefore based on the above-mentioned gaps is:

Can the incorporation of Carbon Fiber Reinforced Polymer (CFRP) and a new chassis design configuration combined with advanced FEA techniques optimize mass efficiency and structural performance of Lunar Zebro to enhance lunar exploration?

For a nano scale rover like the Lunar Zebro, operating under tight mass and volume constraints, the relationship between mass and stiffness becomes extremely critical. The limitations of conventional design practices, particularly under dynamic launch conditions and lunar surface loads, necessitate a targeted investigation. It is within this framework defined by the complexity of multi-axial loading, material anisotropy, and geometric sensitivity that a dedicated research effort becomes essential to guide the next stage of chassis development.

2. Research Approach

2.1. Motivation

A unique engineering challenge in the structural design of the lunar rover chassis is to minimize mass and accommodate manufacturability constraints while achieving high stiffness and reliability under extreme multiaxial loading. The isotropic material behaviour of earlier Aluminium-based designs limits directional stiffness tuning in the case of Lunar Zebro.

The potential of anisotropic layups to provide mechanical advantage through customized stiffness distribution is highlighted by recent trends in composite integration across space-grade platforms. However, failure prediction and laminate optimization become more complex as a result of this design freedom. Analytical simplifications alone are insufficient to address these issues, particularly in thin-walled geometries that are susceptible to both local interlaminar effects and global deformation. This calls for a high-fidelity simulation-driven investigation of material and geometric configurations that takes into account damage initiation and through-thickness stress evolution in addition to in-plane stiffness under realistic boundary conditions. Redistributing stress concentrations, increasing torsional rigidity, and attaining structural compliance without needless mass penalties are further benefits of design modifications like switching from boxes to geometrically contoured profiles or adding reinforcements.

The loading environment drives the design considerations specific to mission. Inertial forces and high-frequency vibrations that are transmitted from launch vehicle are the responsible for the structural loads on lunar rover chassis during the launch phase. Additional stresses are created by the mounting zones by imposing localized boundary conditions and mechanical interface of chassis with the lander therefore, it is required to account for all the mentioned conditions and thresholds for getting the optimum chassis configuration.

2.2. Objective

By improving strength and optimizing mass, this study compares metallic and fiber-reinforced composite configurations in an effort to optimize the Lunar Zebro chassis mechanical performance under launch and operating load. Among the main goals are:

- Comparing the mass-to-stiffness ratio, structural integrity, and buckling resistance of CFRP-based configurations to those of traditional Aluminium.
- Examining how the stacking order and ply orientation affect the anisotropic response of thin-walled composite structures to bending, shearing, and axial loads.
- Determining the limiting factors in composite performance by assessing failure criteria like the Tsai-Wu index and delamination risk.
- Utilizing a fixed chassis layout to quantify displacement, stress distribution, and eigenfrequency response for various material-stack configurations.

The study's ultimate goal is to develop a chassis configuration that maximizes directional stiffness, satisfies launch survival requirements, and offers mass efficiency appropriate for small-scale lunar deployment.

2.3. Proposal

A multi-resolution finite element simulation framework created in COMSOL Multiphysics is used in the suggested method, which aims to characterize structures at two successive levels:

2D flat plate models with representative boundary conditions and a variety of stacking sequences ([0/90], [0/90/0], [0/90/90/0], and [0/45/–45/0]), were used to examine the directional stiffness and failure evolution at interface levels. Another step is determining the thickness that offers the best strength.

3D box-level simulations with acceleration-aligned constraints, mounting interfaces, and realistic leg-loading scenarios that mimic launch configuration. Here, ribbed areas, local curvature, and extrusion effects are taken into consideration when assessing structural performance.

The Tsai-Wu failure index (σ), maximum and displacement, first eigenmode frequency, and possible interlaminar delamination under Mode I and Mode II stress states are among the important mechanical metrics that can be extracted from these calibrated simulation models. This simulation approach co-optimizes the laminate configuration, material, and geometry. Without going over mass budget or complexity limits, the results will help determine the best ply orientations for each structural region, location-specific thickness refinement, and internal reinforcement techniques.

2.4. Methodology

The numerical study resolves laminate stress and failure propagation in composite laminates using a layered shell-based finite element method. The following steps make up the methodology:

1. Material definition and calibration: Engineering data from the literature is used to implement the orthotropic elastic properties for CFRP (E_1, E_2, G_{12}, v_{12}).
2. Ply layup modelling: COMSOL's Layered Shell interface is used to model every composite configuration. This enables the tracking of in-plane and transverse stress tensors at the mid- and interface planes, as well as the definition of individual ply angles.
3. Boundary condition assignment: To replicate the mechanical conditions corresponding to the launch stack and post-landing surface deployment, the chassis is restricted at specific area on the top wall. Based on the estimated inertial force distribution from launch accelerations (10g body load), vertical loads are applied.
4. Evaluation of failure criteria: Tsai-Wu and maximum stress criteria are assessed for each ply. To capture the beginning and progression of through-thickness failure, fracture energy-based delamination models are used to track the interface damage variable.
5. Design convergence and optimization: The final design choice is predicated on a configuration that ensures Eigen frequency above 100 Hz and Tsai-Wu index < 1.0 for all plies while minimizing mass. The final iteration is guided by parametric studies on layup symmetry and wall thickness.
6. Comparative performance analysis: For every configuration, key metrics such as failure index, peak stress, Eigen frequency, and maximum displacement are extracted. To determine performance trade-offs, results are plotted against mass estimates.

   This methodology guides the development of a mass-optimized and structurally sound lunar rover chassis by providing a mechanical understanding of the interactions.

3. Chassis Surface Modelling

A plate model was developed to assess CFRP and Aluminium's performance under body loading when represented as thin-walled chassis surfaces. To reflect realistic fabrication limits, failure criteria, and structural performance under a 10g gravitational body load in the Z-direction, a comparative displacement study was carried out on plates of different thicknesses.

3.1. Stress Analysis of Aluminium Plate under Body Load

To assess the structural performance of Aluminium under high-load conditions, a series of simulations were performed on flat Aluminium plates with dimensions 200 mm × 140 mm, varying only in thickness: 2 mm, 1.5 mm, and 1 mm. The goal was to determine the stress response under a body load simulating launch acceleration of 10g and to evaluate whether Aluminium remains structurally safe at reduced thickness. A 40 mm × 40 mm fixed square region was used to constrain the plate in the center, simulating the mounting arrangement in the rover design as shown in figure 14. In the Z-direction, a constant gravitational body load was applied to simulate the load encountered during lunar launch.

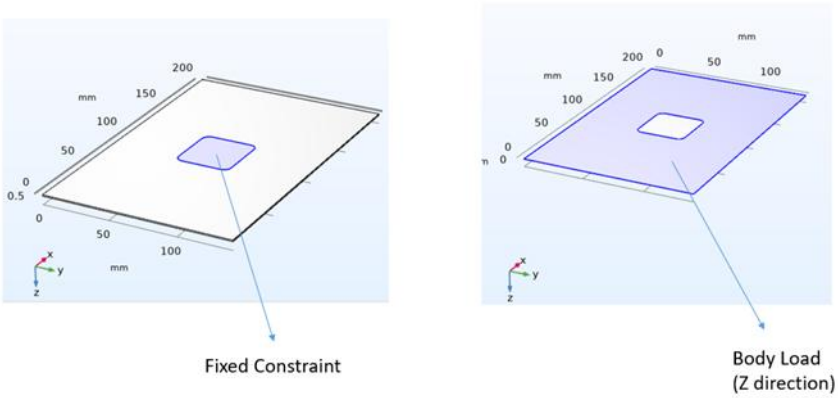

Figure 14: Boundary conditions showing fixed constraint (left) and body load (right)

Von Mises stress concentrations around the fixed constraint are shown by the simulation results. Because of the decreased bending stiffness, the maximum stress levels increase dramatically as the plate thickness decreases. The stress distributions for the three thicknesses are displayed in figure 15.

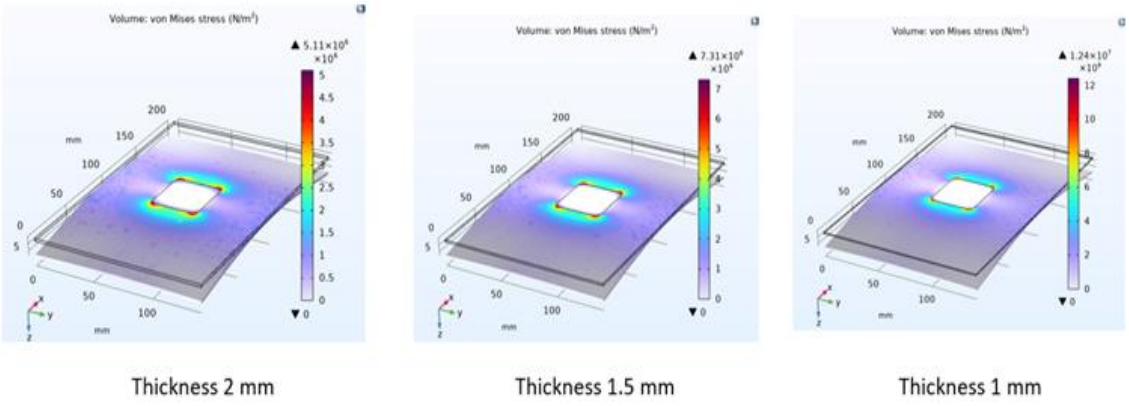

Figure 15: Von Mises stress distribution in Aluminium plates under 10g body load for thicknesses of 2 mm, 1.5 mm, and 1 mm (left to right).

According to [17] the yield strength of pure Aluminium is 7–11 MPa. The strength of pure, easily machined, and cast material. The distribution of stress changes significantly as the thickness of the Aluminium plate decreases. The stress is still minimal and uniformly

distributed throughout the plate at a thickness of 2 mm. Higher stress levels result from cutting the thickness to 1.5 mm, especially in the vicinity of the central constraint's edges. Von Mises stress increases dramatically at a thickness of only 1 mm, causing localized yielding that indicates the beginning of material failure. The maximum von Mises stress values from each simulation are compiled in the table below and contrasted with the approximate yield strength of pure Aluminium (approximately 11 MPa). The stress exceeds the yield point at 1 mm thickness (12.4 MPa), indicating that plastic deformation would take place under load. An interpretation of whether the material stays within the elastic range is also included.

Plate Thickness	Max von Mises Stress (MPa)	Comparison to Yield Strength (Pure Al ≈ 11 MPa)	Interpretation
2 mm	5.11	Below Yield	Safe under load (Elastic range)
1.5 mm	7.31	Below Yield	Still safe (Elastic, nearing yield)
1 mm	12.4	Exceeds Yield	Plastic deformation begins

Table 2. Maximum von Mises stress and interpretation for different Aluminium plate thicknesses

3.2. Failure criteria check for CFRP

The same body load conditions (10g) that led to the failure of the Aluminium plate at 1 mm are used in this section to assess the structural performance of a Carbon Fiber Reinforced Polymer (CFRP) plate with a total thickness of 1 mm. Verifying whether CFRP retains integrity across all layers and interfaces without going over failure indices or delaminating is the aim. To accurately depict individual plies and their orthotropic behaviour, layered shell mechanics was used to model a CFRP plate with dimensions of 200 mm × 140 mm. The constraint condition, which was a 40 mm×40 mm fixed square region at the center with a uniform body load in the Z-direction simulating launch acceleration, was the same as in the Aluminium analysis. The laminate used in this analysis is made up of five unidirectional plies, each of which has a thickness of 0.2 mm as shown in figure 16. The total thickness of the laminate is 1 mm. The fibers are oriented along the main structural axis, and the stacking sequence is [0/0/0/0/0]. This stacking represents a conservative load-bearing scenario for launch stress since it maximizes bending stiffness in a single direction.

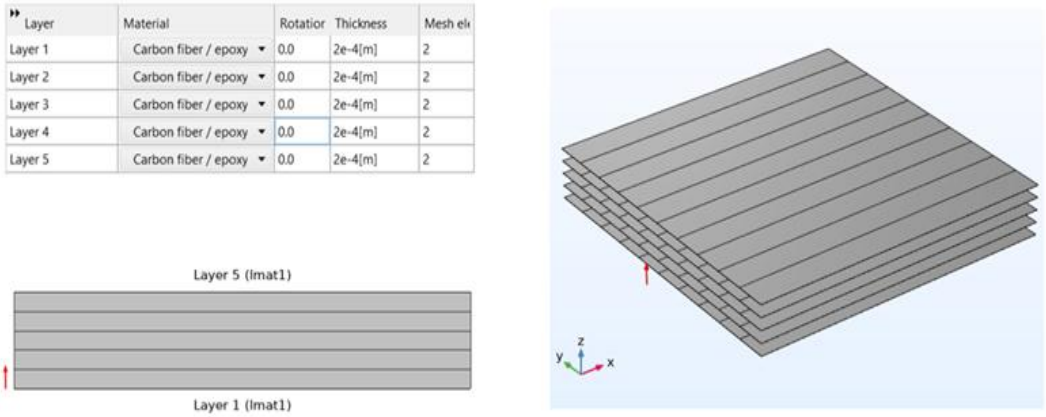

Figure 16: Laminate structure and material input table for 1 mm CFRP with five 0° plies

3.2.1. Delamination Analysis using Cohesive Zone Modelling

To examine interlaminar strength, a cohesive zone model (CZM) was used at ply interfaces. Parameters required for the FEA modelling of CZM such as tensile strength, shear strength,

and fracture energy release rates were assumed based on standard CFRP-epoxy values. The purpose of the cohesive elements is to ensure that the elements of the elastic bodies adjacent to the fracture interfaces experience the correct boundary tractions during the evolution of delamination. [18]

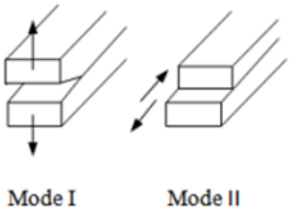

Figure 17**:** Mode I and Mode II of the Delamination as modelled in CZM

Crack surfaces separate perpendicular to the interface in Mode I (Opening Mode) and in Mode II (Sliding Mode), in-plane shearing occurs when crack surfaces slide over one another.

Tensile energy release rate is the energy needed to delaminate under tension (normal direction fracture toughness), while shear energy release rate is the energy needed to propagate delamination in sliding (shear direction fracture toughness). [19] Tensile strength is the maximum normal stress the interface can withstand before damage begins (Mode I), and shear strength is the maximum shear stress before the interface begins to degrade (Mode II). Each interface's condition is indicated by the damage variable. Table 3 provides an interpretation and visual representation of the damage variable under delamination:

Damage Value	State of the Interface	Explanation
0	Bonded	No degradation has occurred; the interface is intact and transferring load normally
1	Delaminated (Failed)	Interface has completely failed; no load transfer across the interface

Table 3. Damage variable under delamination

Figure 18: Damage plot showing no delamination (damage = 0 across all interfaces)

3.2.2. Tsai-Wu Failure Analysis (Ply-Level Integrity)

One of the most popular tensor-based failure theories for anisotropic composite materials is the Tsai-Wu failure criterion. To ascertain whether any ply in a laminated composite is likely to fail, it provides a scalar failure index that takes into consideration the combined effects of normal and shear stresses on various material axes. When assessing fiber-reinforced composites, such as CFRP, where strength varies significantly along and across the fiber directions, this method is extremely helpful. The orthotropic stress components and material strength limits were used to calculate the Tsai-Wu failure index for each of the five layers. The

general Tsai-Wu failure criterion for an orthotropic lamina under plane stress can be expressed mathematically as follows:

$$F_1\sigma_1 + F_2\sigma_2 + F_{11}\sigma_1^2 + F_{22}\sigma_2^2 + F_{66}\tau_{12}^2 + 2F_{12}\sigma_1\sigma_2 = 1 \quad (1)$$

where τ12 is the in-plane shear stress and σ1 and σ2 are the normal stresses in the transverse and local fiber directions, respectively. (Ref: Design and manufacture of a high-G unmanned aerial vehicle structure). σ1 = lshell.sx, σ2 = lshell.sy, and τ12 = lshell.sxy in COMSOL. The Tsai-Wu coefficients F1, F2, F11, F22, F66, and F12 are computed as follows:

$$F1 = 1/X_t + 1/X_c \quad (2)$$

$$F11 = (-1)/(X_t X_c) \quad (3)$$

$$F2 = 1/Y_t + 1/Y_c \quad (4)$$

$$F22 = (-1)/(Y_t Y_c) \quad (5)$$

$$F1 = 1/S^2 \quad (6)$$

$$F1 = (-0.5)/\sqrt{X_t X_c Y_t Y_c} \quad (7)$$

Here, Yt and Yc represent the tensile and compressive strengths in the transverse direction, while Xt and Xc represent the tensile and compressive strengths in the fiber direction, respectively. S is the composite lamina's shear strength.

Table 4 provides an interpretation of the Tsai-Wu index. [20]

Tsai-Wu Index Value	Meaning	Implication
< 1.0	Safe – All stress components are within allowable limits	Design is structurally sound under current load
= 1.0	Onset of Failure – First ply failure is imminent	Indicates the critical load or limit state
> 1.0	Failure – Stress has exceeded strength limits	Lamina has failed; redesign or reduce load

Table 4. Tsai-Wu index

The formula for the 200 x 140 plate under the same loading conditions was used to calculate the Tsai-Wu index. The laminate's maximum Tsai-Wu index, which is the top layer out of the laminate, is displayed in the figure below.

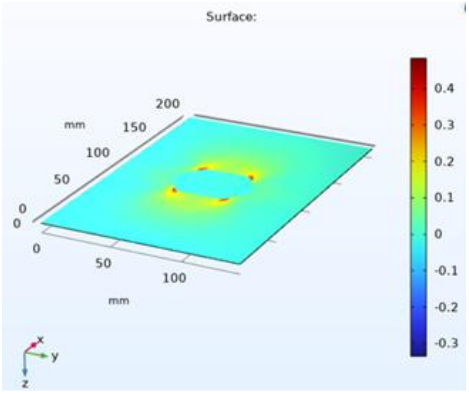

Figure 19: Tsai-Wu surface plot for CFRP plate showing safe stress regions below failure limit.

The plot shows that the Tsai-Wu index of 0.48 is less than 1, indicating that the ply is safe. This was a layer 5 plot. The index is calculated in COMSOL for each ply as shown in table 5.

Layer number	Tsai-Wu index
1 (bottom layer)	0.48301
2	0.48318
3	0.48327
4	0.48331
5 (top layer)	0.48350

Table 5. Tsai-Wu index of CFRP plate

All plies are structurally safe under the applied body load, according to the Tsai-Wu index table. The top and bottom layers are under tension and compression, respectively. Through thickness, the stress changes. The plate's bottom surface compresses (compression) while its top surface stretches (tension). The plate behaves as though it is under bending even though it is under body load because of the central fixed patch. If Xt < Xc, the same stress in tension is more critical (produces higher Tsai-Wu) than in compression. Compared to Aluminium at the same thickness, CFRP was within safe bounds at 1 mm, as determined by failure criteria.

3.3. Comparative analysis based on displacement and mass

To confirm CFRP as a safer and more structurally sound option for lightweight applications like the lunar rover chassis, a displacement analysis at 1 mm is now necessary. Both CFRP and Aluminium plates were examined under a constant 10g body load with central fixed constraints to evaluate structural viability for spaceborne applications. To examine the effect on displacement, the thickness was changed from 2 mm to 1 mm while the plate's dimensions stayed fixed at 200 mm × 140 mm. For Aluminium plates of varying thicknesses, the displacement fields show a sharp increase in deflection with decreasing thickness as shown in figure 20.

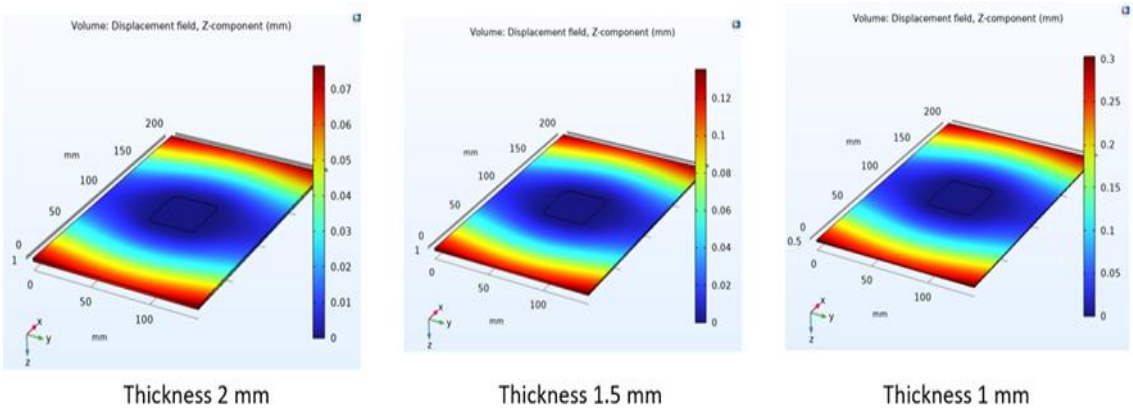

Figure 20: Displacement plot of Aluminium plates of varying thicknesses

The CFRP plates, modelled using layered shell mechanics with [0/0/0/0/0] layup, show superior resistance to displacement as shown in figure 21.

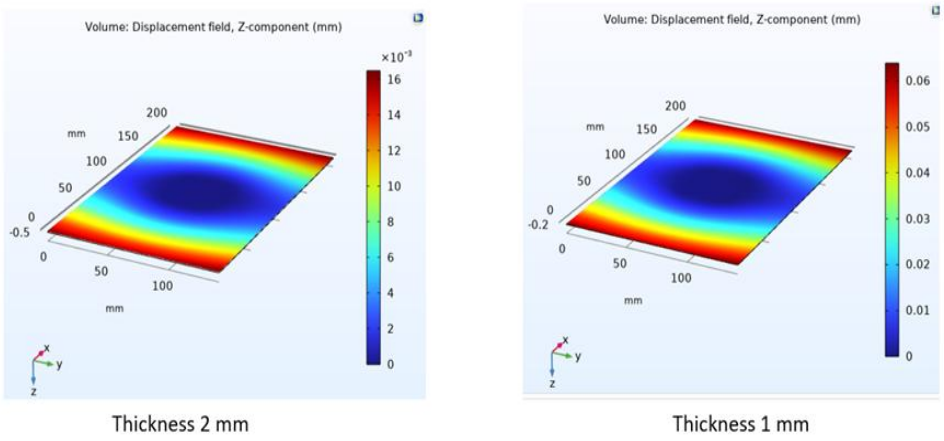

Figure 21: Displacement plot of CFRP plates of varying thicknesses

The displacements of CFRP and Aluminium at various thicknesses are contrasted in table 6. In CFRP simulations, the delamination setting was turned off to guarantee an equitable displacement comparison between CFRP and Aluminium. When damage is zero, this prevents cohesive interface elements from introducing artificial compliance.

Material	Thickness	Displacements (mm)
Aluminium	2 mm	0.07
Aluminium	1.5 mm	0.13549
Aluminium	1 mm	0.30307
CFRP	2 mm	0.01649
CFRP	1 mm	0.06395

Table 6. CFRP and Aluminium at various thicknesses

CFRP at 1 mm maintains structural stiffness with a displacement of 0.06395 mm, which is less than even Aluminium at 2 mm, whereas Aluminium at 1 mm experiences excessive deflection (0.30307 mm). The CFRP laminate showed less displacement under body load than a 2 mm thick Aluminium plate, even though it was only 1 mm thick. This demonstrates the fiber-

reinforced composites' superior stiffness-to-mass efficiency. The bending stiffness, which is influenced by the in-plane modulus (E_1, E_2, etc), laminate thickness, layup symmetry, and ply stacking, provides resistance even when the load is in the Z direction. The benefits of using CFRP are further enhanced by its lower mass.

Property	Aluminium	CFRP
Mass	Higher	Lower
Max Displacement	Higher	Lower
Failure Mode	Yielding (Von Mises)	Delamination/ Tsai-Wu

Table 7. Material comparison based on mass, displacement, and failure modes

As shown in table 7, at reduced thickness, CFRP performs noticeably better than Aluminium in terms of strength and stiffness. It is a strong, lightweight substitute for space-grade structural panels where mass, safety, and performance are crucial because it maintains low displacement under 10g load, exhibits no ply failure according to Tsai-Wu, and stays bonded across all layers.

3.4. Optimization Strategy for Ply Design

The subsequent stage of this investigation entailed a focused design optimization of the CFRP laminate, building on the previous results that showed CFRP's superior structural performance over Aluminium under the same loading conditions. To preserve structural consistency and practical manufacturability in this situation, some design elements were kept constant. Carbon Fiber Reinforced Polymer (CFRP) was specifically chosen as the material because of its high stiffness-to-weight ratio and resistance to delamination and yielding. To replicate the realistic chassis wall design, the geometry was kept as a flat rectangular plate, and all laminates maintained stacking symmetry to guarantee balanced bending response.

Once these factors were established, the optimization concentrated on two crucial design factors: the overall thickness of the laminate and the orientation of the plies. To improve the laminate's resistance to multi-axial loading, control bending stiffness, and redistribute stress, individual plies' orientation is crucial. The goal was to find a configuration that minimized Z-direction displacement under a 10g body load without sacrificing failure safety by experimenting with different fiber angles, such as [0/90/90/0], [0/45/-45/0], and other symmetric layups. After determining the ideal orientation, the laminate's thickness was gradually decreased layer by layer using a parametric sweep. To make sure structural safety was maintained, the Tsai-Wu failure index and delamination damage were closely monitored at every stage. To confirm that the laminate remained more rigid than the 1.5 mm thick Aluminium plate, displacement was also tracked.

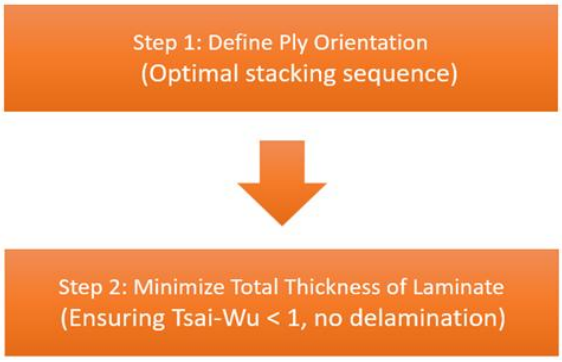

Figure 22: Optimization flow

This method made it possible to determine the CFRP configuration that was the lightest and thinnest while maintaining structural integrity, providing better performance than all tested Aluminium variants and thicker CFRP plate.

3.4.1. Ply Orientation Modelling

First, a classification of typical laminate stacking sequences was examined to direct the design process for the best CFRP layups. These common orientations provide different trade-offs in terms of stiffness, strength, and directional load distribution. These include unidirectional, cross-ply, angle-ply, quasi-isentropic, and multidirectional layups. [21]

These orientations and the stacking notations that correspond to them are described in Table 8. The mechanical performance of these layups under the same loading and boundary conditions was evaluated using simulation.

Example	Laminate Stacking Sequence
Unidirectional	$[0/0/0/0/0/0] = [0_6]$
Cross-ply symmetric	$[0/90/0/90/0] = [0/90]_S$
Angle-ply symmetric	$[45/-45/-45/45] = [45/-45]_S = [\pm45]_S$
Angle-ply asymmetric	$[30/-30/30/-30/30/-30/30/-30] = [30/-30] = [\pm30]_4$
Quasi isentropic	[0/45/-45/90]
Symmetric Quasi isentropic	$[0/45/-45/90/90/-45/45/0] = [0/\pm45/90]_S$
Multidirectional	[0/+45/30/-30/45]

Table 8. Typical Types of Orientations and Their Laminate Sequences of Stacking

A displacement comparison was carried out for every configuration under a constant total thickness of 1 mm to assess how these layups behave in real-world situations. The symmetric cross-ply layup [0/90/0/90/0] produced an even smaller displacement of 0.06388 mm, as indicated in Table 9, whereas the unidirectional layup $[0]_5$ produced a greater displacement of 0.06395 mm. This proved that adding orthogonal fibers enhances load distribution while maintaining rigidity.

In contrast, angle-ply layups like [45/-45/45/-45/45] had a much larger displacement of 0.11871 mm. This suggests that although angle-ply configurations provide better shear resistance in-plane, they also decrease bending stiffness along the principal axes. Comparably, hybrid configurations like [0/30/60/-30/-60] or [90/0/0/-45/45] provided intermediate displacements, while asymmetric configurations like [30/-30/30/-30] demonstrated a moderate increase (0.08993 mm).

Layup	No. of Layers	Displacement (mm)
$[0]_5$	5	0.06395
[0/90/0/90/0]	**5**	**0.06388**
[45/-45/45/-45/45]	5	0.11871
[30/-30/30/-30]	4	0.08993
[0/30/60/-30/-60]	5	0.08646
[90/0/0/−45/45]	5	0.0857

Table 9. Displacement Comparison for Different Layups at 1 mm Thickness

In addition to maintaining the lowest displacement, these results clearly showed that cross-ply symmetric layups, like [0/90/0/90/0], achieved balanced and symmetric architecture, which is essential for out-of-plane stiffness. If the overall laminate thickness stays at 1 mm, this prompted a concentrated investigation into the effects of layer count in cross-ply configurations on performance. The impact of changing the number of layers in cross-ply laminates while maintaining a constant thickness is shown in Table 10. The 4-layer configuration [0/90/90/0] displayed the lowest displacement of 0.06384 mm, though the difference was slight, whereas a 2-ply [0/90] laminate and a 5-ply [0/90/0/90/0] laminate both produced larger displacement of about 0.06388 mm.

Layup	No. of Layers	Balanced	Symmetric	Displacement (mm)
[0/90]	2	No	No	0.06388
[0/90/0]	3	No	Yes	0.064
[0/90/90/0]	4	Yes	Yes	0.06384
[0/90/0/90/0]	5	No	Yes	0.06388

Table 10. Effect of Number of Layers in Cross-Ply Layups (Total Thickness = 1 mm)

This finding implies that stiffness performance is more significantly influenced by the laminate's symmetry and balance than by the quantity of layers. Notably, the symmetrical and balanced 4 ply configuration [0/90/90/0] offers the best mechanical behaviour under the applied loading.

By assessing both ply-level failure and interlaminar integrity, the safety of every ply orientation configuration tested during the optimization phase was confirmed under a 10g body load. With delamination modelling enabled, cross-ply laminates like [0/90/0/90/0], [0/90/90/0], [0/90/0], and [0/90] were all simulated and evaluated. No single ply went over its permitted limit in any of the cases where the Tsai-Wu failure index stayed below 1. Furthermore, the damage variable was zero for all ply interfaces, indicating that even with high accelerative body loads, no delamination had begun. These findings confirmed that every tested orientation was capable of safely distributing the applied loads, confirming their suitability as lightweight structural design candidates. The subsequent phase concentrated on lowering the overall laminate thickness while preserving this margin of structural integrity after the safe ply orientations were established.

3.4.2. Thickness Optimization Following Ply Orientation

Following the selection of the best ply orientation to reduce displacement and guarantee structural safety, the subsequent stage concentrated on lowering the overall laminate thickness to save more mass without sacrificing performance. Because they offered good Tsai-Wu indices and delamination resistance under a 10g body load, the cross-ply configurations ([0/90], [0/90/90/0], etc.) found in the orientation study were kept for this stage. Finding the minimum CFRP thickness that still met the following crucial design requirements was the goal: low displacement (less than or equal to Aluminium), a Tsai-Wu failure index below 1, and no delamination damage. To cover a range of total thickness values from 1 mm to 0.6 mm, a number of simulations were run with different plies and individual ply thicknesses. The simulation results for various laminate configurations are displayed in Table 11, along with important output metrics like maximum displacement, Tsai-Wu index, and delamination damage status. To confirm the interfacial strength, delamination was turned on in every simulation.

Total Thickness (mm)	Ply Count	Ply Thickness (mm)	Max Displacement (mm)	Max Tsai-Wu Index	Damage = 0
1.0	5	0.2	0.06388	0.48746	Yes
1.0	4	0.25	0.06384	0.44292	Yes
0.9	5	0.18	0.0787	0.49997	Yes
0.9	4	0.225	0.07862	0.46651	Yes
0.8	4	0.2	0.09926	0.4877	Yes
0.6	3	0.2	0.17558	0.48722	Yes
0.6	2	0.3	0.17559	0.38246	Yes
0.7	4	0.175	0.12932	0.50275	Yes
0.7	3	0.233	0.12935	0.45811	Yes
0.69	**4**	**0.1725**	**0.13306**	**0.50489**	**Yes**

Table 11. Thickness Optimization Results for CFRP Cross-Ply Laminates

Even at lower thicknesses, certain configurations maintained their structural integrity. The 0.69 mm laminate with four plies of 0.1725 mm each was particularly intriguing. A displacement of 0.13306 mm was obtained with this configuration, which is less than the 0.13549 mm for Aluminium at 1.5 mm thickness. Additionally, there was no delamination damage and the Tsai-Wu index was 0.50489, which is safely below the failure threshold. At 0.6 mm plate thickness, four plies result is not mentioned in the table 10 due to convergence issue caused by high non-linearity because of the very small ply thickness of 0.15 mm. A quadratic regression was fitted to the displacement vs. thickness data to capture continuous trend observed in the simulation results. The relationship showed a smooth curvature rather than linear or abrupt where the displacements decreased with increasing thickness and then the drop in displacement would keep on becoming lower in magnitude. The characteristics were suited for a second order polynomial fit. It was confirmed that this was the lowest CFRP thickness that could match or surpass Aluminium's stiffness under body load when the polynomial curve intersected the Aluminium displacement benchmark (0.13549 mm) at a thickness of 0.69 mm, as seen in Figure 23.

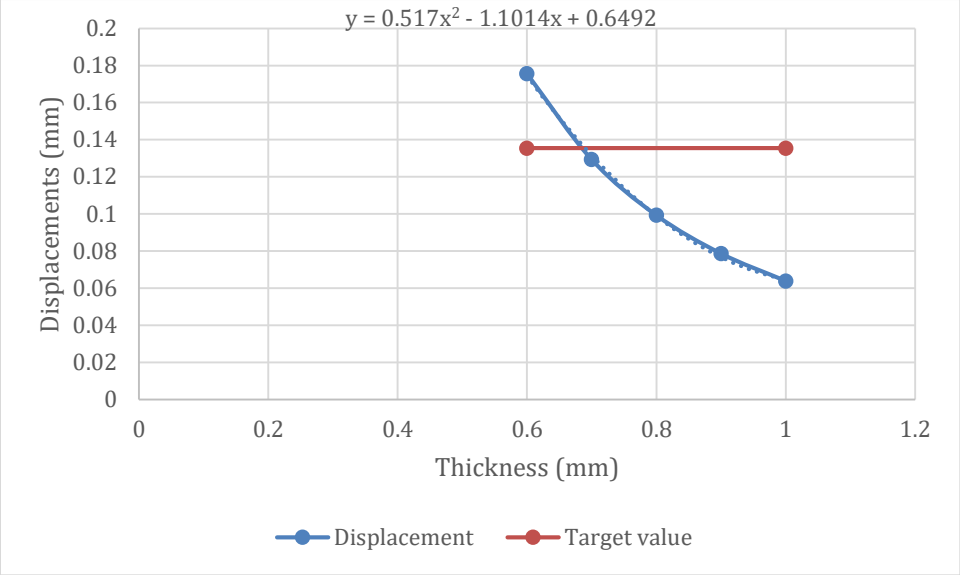

Figure 23. Displacement vs. Thickness Plot for Cross-Ply CFRP Laminates for locating the thickness at Aluminium displacement benchmark (0.13549) through intersection of this target value with the displacement curve

According to this research, CFRP not only satisfies the stiffness of 1.5 mm thick Aluminium at a critical thickness of 0.69 mm, but it also offers a lighter (a 72.74% mass reduction as compared to 1.5 mm Aluminium plate) and structurally safer substitute (refer to appendix for the mode shapes). To simulate the entire structure and analyze system-level performance, this configuration will be maintained in the full chassis model (a box), which will be built from six such plates.

4. Chassis Box Modelling and Material Comparison

The next step of the simulation process was creating and examining a complete box-shaped chassis model to assess the optimized CFRP layups' practicality. This box, which was made of six plates with the ideal ply configuration [0/90/90/0] and each wall thickness of 0.69 mm, represented a simplified geometry of the Lunar Zebro's structural enclosure. In COMSOL, the box is represented as a combination of six layered shells. The box's external measurements were 200 mm × 140 mm × 60 mm [22], and the top central area, which served as the mounting interface, was subject to a fixed constraint of 40 mm × 40 mm. Consistent with previous plate analysis, a 10g launch acceleration scenario was simulated by applying a uniform body load in the Z-direction.

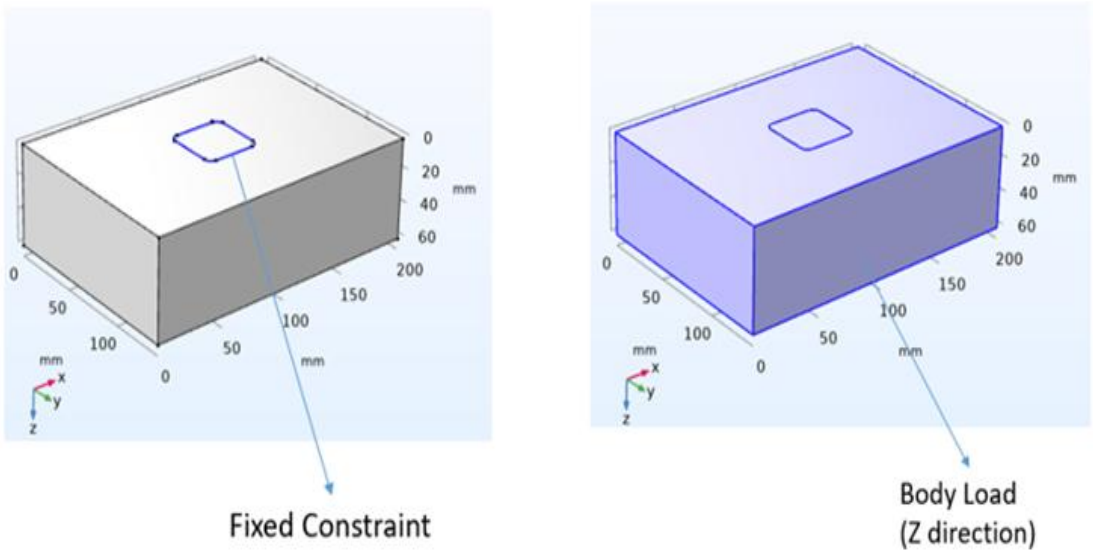

Figure 24: Boundary conditions showing fixed constraint (left) and body load (right)

4.1. Simulation Setup and Workflow

The process started with the definition of geometry, the assignment of materials (CFRP and Aluminium), and structural simulation under two categories: static structural analysis and eigenfrequency analysis, as illustrated in the simulation flowchart (Figure 25). Determining von Mises stress values and displacement under launch-equivalent body loading was the aim of static simulation. The body load in COMSOL was force per unit volume where the load is calculated by Force = mass x acceleration (10 g) / volume. The mass/volume becomes density therefore, Force = 10 x 9.81 x density. The force would be different depending on the material applied to the chassis. To ascertain the natural frequencies of the chassis and evaluate modal safety margins, the eigenfrequency analysis, on the other hand, was carried out with the same fixed constraint but without any external load.

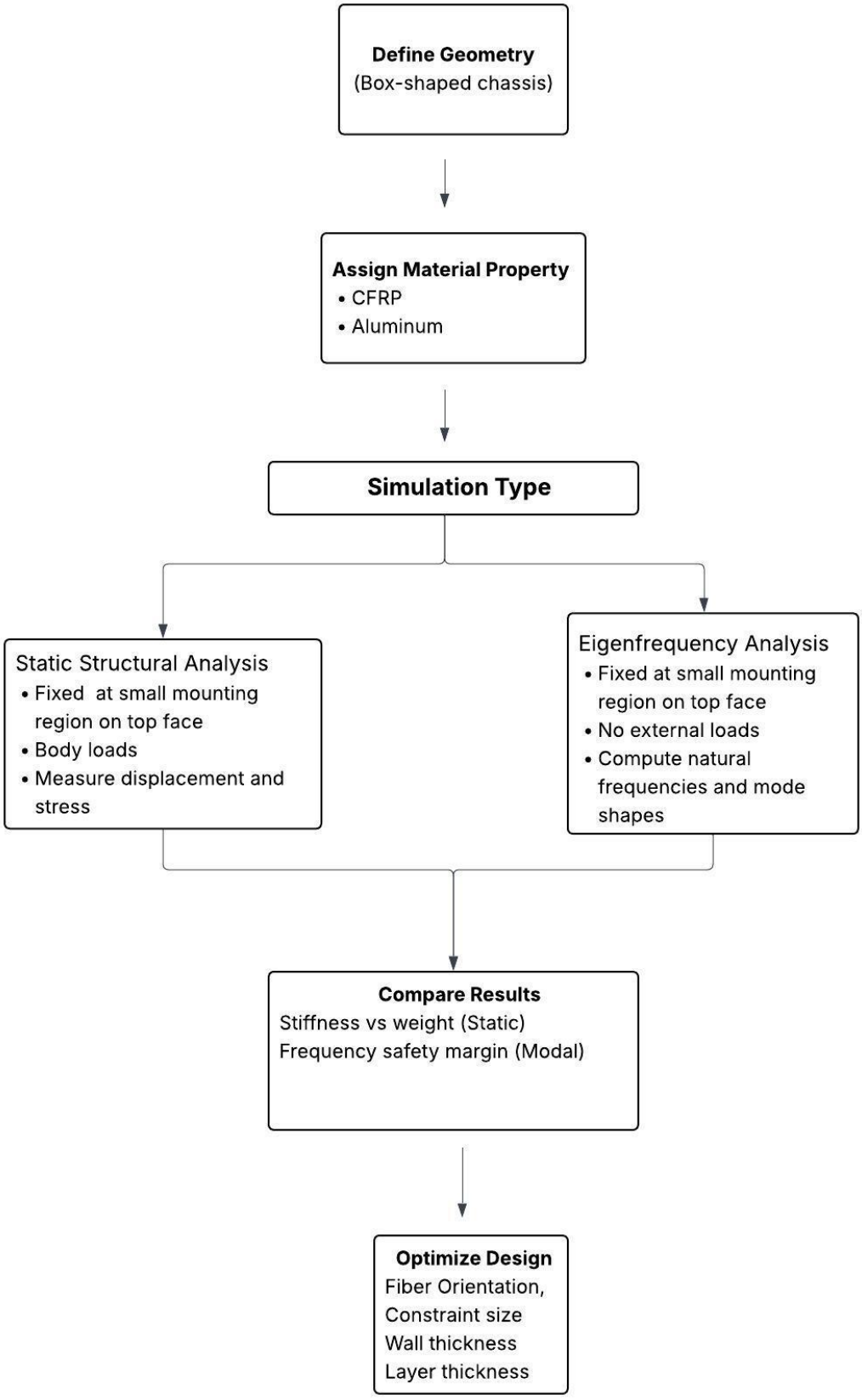

Figure 25: Workflow of developing and analyzing box chassis

4.2. Stress Response and Safety Margin

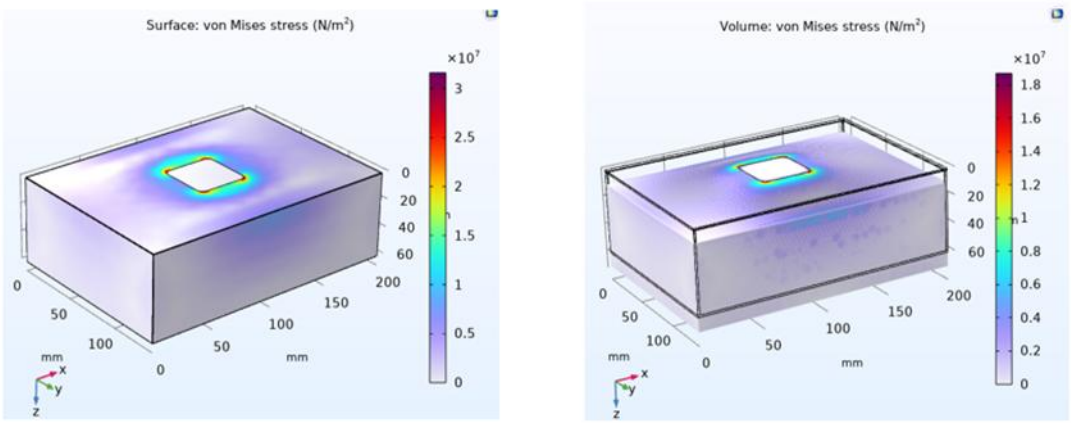

CFRP Aluminium

Figure 26: Von Mises stress distribution in box under 10g body load for CFRP (left) and Aluminium (right)

Under the same loading conditions, stress plots of CFRP and Aluminium box geometries show clear variations in structural behaviour. With a wall thickness of 0.69 mm, the CFRP chassis showed evenly distributed stress that peaked near the central constraint patch. Despite having a thicker 1.5 mm wall, the Aluminium chassis showed a peak von Mises stress of 18 MPa, which is higher than the yield strength of pure Aluminium, which is 11 MPa. Under launch loading conditions, this signals the beginning of plastic deformation and failure. Even when the wall thickness is more than doubled, Aluminium still does not stay within elastic bounds.

4.3. Displacement Analysis

A crucial realization is revealed by additional displacement magnitude comparison. A maximum vertical displacement of 0.18849 mm was experienced by the CFRP box (0.69 mm, [0/90/90/0] layup). Because of its thicker wall, the 1.5 mm thick Aluminium box had a smaller displacement of 0.148 mm, but it still failed under stress. Therefore, CFRP's marginally greater displacement is acceptable. More significantly, CFRP provides superior stiffness-to-weight efficiency by achieving this performance at a significantly lower mass (72% reduction in mass of the box).

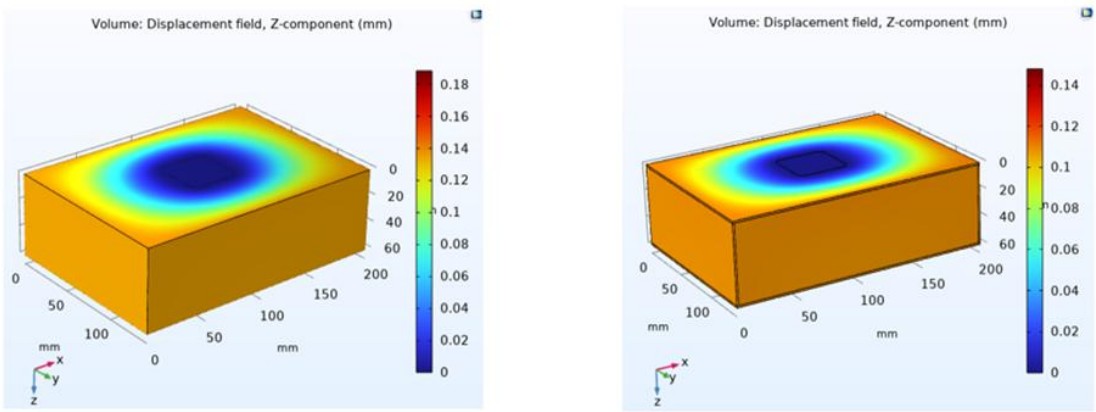

CFRP Aluminium

Figure 27: Displacement plot of CFRP and Aluminium

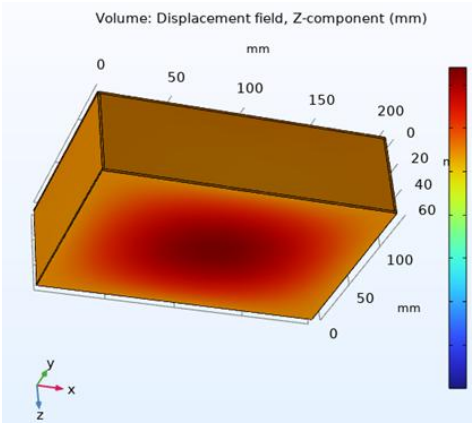

Figure 28. View of Bottom wall

The symmetrical and centrally distributed displacement concentration observed from the bottom wall view validates that the deformation pattern corresponds with the anticipated load transfer from the mounting region.

4.4. Ply Orientation Sensitivity in Thin-Walled Box

A comparative study was carried out on different layup orientations using the same boundary conditions and body load magnitude to fine-tune the structural response of the optimized 0.69 mm CFRP box. The objective was to determine whether small stacking adjustments could improve the overall stiffness response and to investigate how changing fiber directionality impacts displacement behaviour in the complete 3D geometry. The displacements obtained for various layups tested on the 0.69 mm thick box walls are summarized in the table below.

Layup	Displacement (mm)
[0/90/90/0]	0.18849
[0/45/-45/0]	**0.18653**
[90/45/-45/90]	0.18668
[0/0/0/0]	0.18802
[0/60/-60/0]	0.18799
[90/0/-45/45]	0.20500

Table 12. Layer orientation vs displacement in full CFRP box

With a displacement of 0.18653 mm, the layup [0/45/-45/0] outperformed both [0/90/90/0] and [90/45/-45/90] by a small margin among the tested configurations. This showed that adding ±45° plies maintained good flexural rigidity while offering marginal advantages in redistributing shear-induced deformation. The slight variations, however, imply that orientation tuning at this thickness level produces marginal rather than significant improvements. The orientation [90/0/-45/45] resulted in the largest displacement (0.205 mm), likely due to unbalanced axial stiffness and reduced bending resistance along the vertical loading axis. This emphasized the importance of keeping layups balanced to maintain shell behaviour under multi-axial loads.

4.5. Effect of Global Box Orientation with Respect to Body Load

To better understand how directional body loads interact with geometry in various mounting configurations and because of the current uncertainty surrounding the rover chassis' mounting onto the lander, the global spatial orientation of the box chassis was assessed in addition to the local ply orientation. Under vertical (Z-direction) body load, simulations were performed for two rotated box orientations. The goal was to evaluate the effects of box rotation on stress concentrations and deformation areas, especially with regard to leg mounting zones.

The results (Figure 29) show that the second orientation, in which the box was rotated so that the 60 mm height extended along the horizontal axis, resulted in a maximum displacement of 0.177 mm. A smaller maximum displacement of 0.128 mm was observed in the third orientation, which involved rotating along the opposite principal axis. The latter might seem to provide a structural advantage at first. A more thorough examination of the displacement distribution, however, showed a significant issue. In the third orientation, the regions of greatest deformation (shown by red zones on the chassis in displacement plots) were found on the lower part of sidewalls, exactly where the legs would be mechanically connected, even though the global maximum displacement value was lower. Because attaching leg modules in areas experiencing significant deformation would jeopardize both mechanical integrity and performance, there is a risk of structural instability. On the other hand, the original configuration (Orientation 1) showed displacement concentrations at the bottom face far from the leg attachment points on the vertical walls, despite having a slightly higher displacement (0.188 mm for [0/90/90/0]). Because of this, it is the most practical orientation for preserving mechanical isolation between flexible deformation zones and crucial mounting interfaces.

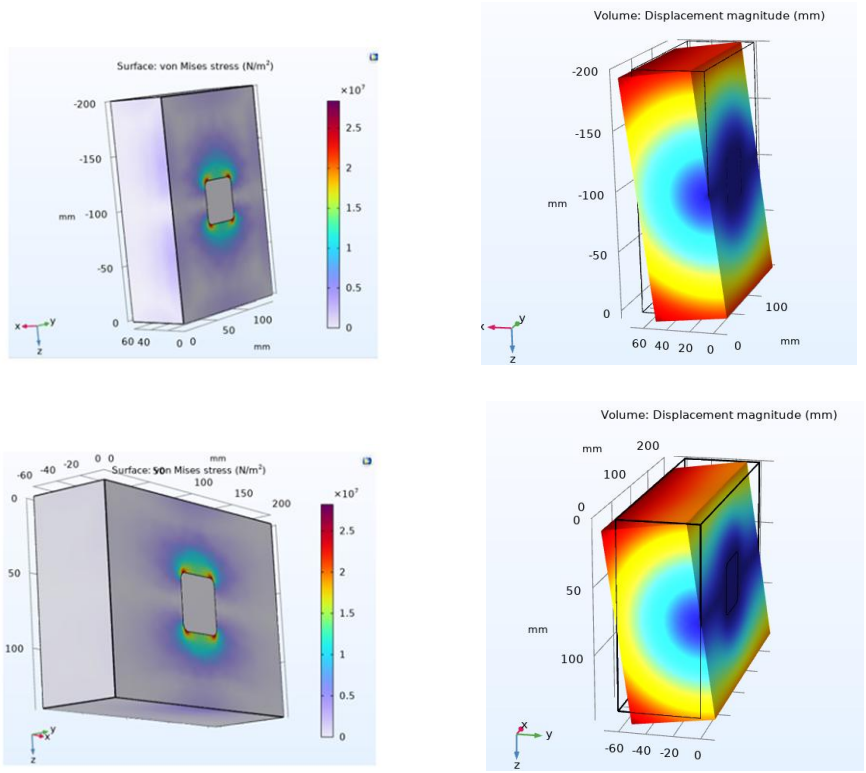

Figure 29: Stress plot and Displacement Magnitude plot of Orientation 2 (top) and Orientation 3 (bottom) of the cuboid chassis

4.6. Modal Performance and Constraint-Size Optimization

The thin-walled CFRP design was obviously preferred by the static results, but the chassis would still need to withstand the harsh vibrational spectrum of launch. To prevent primary launch harmonics from triggering resonant responses, SpaceX advises that structures' first natural frequency be kept comfortably above 100 Hz. [23] In order to better represent the mounting region used in the current Lunar Zebro configuration, an eigenfrequency analysis was performed on the 200 × 140 × 60 mm box, first using the 40 × 40 mm mounting patch used throughout the static work and then using an enlarged 68 × 68 mm patch which is the dimension of original chassis design used in Lunar Zebro.

The 0.69 mm walls in the smaller patch generated a first mode at 65.9 Hz, which increased to 93.9 Hz when the wall thickness was increased to 1 mm (refer to the appendix). Stiffness is determined as much by how the box is gripped as by how thick its walls are, as even the thicker shell stayed just below the desired threshold. The first natural frequency increased to 114.68 Hz and all subsequent modes also shifted upward when the constraint was widened to 68 × 68 mm (Table 13) while maintaining the lightweight 0.69 mm skin and the [0/45/-45/0] lay-up that had worked best in the previous section. Therefore, without the mass penalty that would have been imposed by a global thickening, this one geometric change guaranteed a clean modal margin. Refer to the appendix for the mode shapes.

Mode	CFRP 0.69 mm (Hz)
1	114.68
2	182.23
3	209.26
4	469.61
5	661.19
6	1002.6

Table 13. First six modal frequencies of the CFRP box with 68 mm × 68 mm square constraint

4.7. Consolidated Design Definition

Thus, a single, self-consistent set of design parameters emerged from the combined static, ply-orientation, and modal studies:

- Overall geometry: 200 mm × 140 mm × 60 mm upright box.
- Material system: CFRP laminate [0/45/-45/0].
- Wall thickness: 0.69 mm (four plies of 0.1725 mm each).
- Mounting interface: enlarged 68 mm × 68 mm square patch on the top face

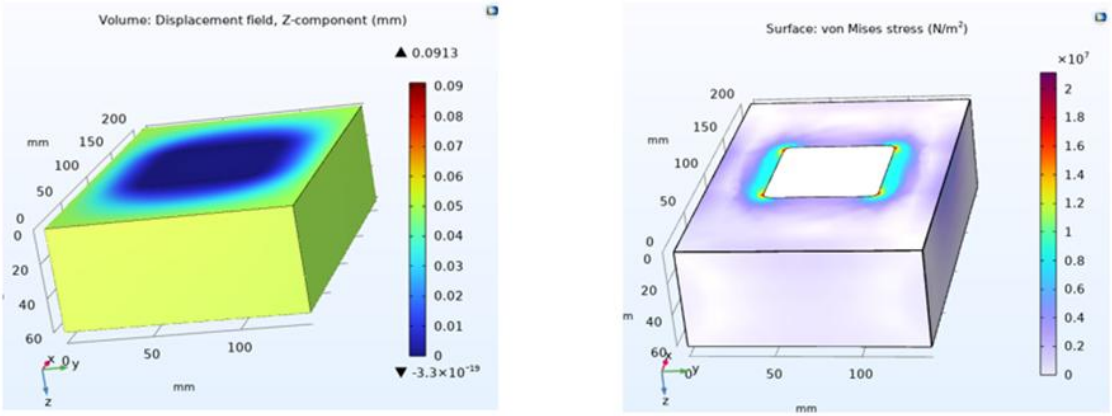

Figure 30: Displacement (left) and stress response (right) of the optimized CFRP chassis under 10g body load (Z-direction)

A full-body simulation of the optimized CFRP chassis with the chosen parameters was used to validate the final configuration after the consolidated design definition. The maximum Z-direction displacement of 0.0913 mm is symmetrically located close to the center of the bottom face, according to the displacement simulation. With no undue deflection along the sidewalls or leg attachment zones, this localized deformation pattern suggests a load transfer that is evenly distributed (Figure 30, left). A qualitative view of the stress concentrations throughout the box's exterior can be seen in the corresponding von Mises stress distribution (Figure 30, right).

In terms of material efficiency, the CFRP chassis total mass in this configuration was determined to be **106.86 grams**, which is a significantly better result when compared to the baseline Aluminium box weight of 384 grams.

5. Design

Following a series of plate and box levels that demonstrated CFRP's superiority, focus shifted towards the chassis geometric design. The final performance of the chassis would be equally determined by the design objective, layout constraints, design adaptability, chassis function, and design parameters under launch and operational stresses, even though the material optimization provided a structurally sound foundation. A more performance-focused definition of the Lunar Zebro chassis was made possible by this optimization strategy. Optimizing the mass and stiffness of the rover's chassis, which bears the majority of its weight, was the primary objective of this phase. This phase sought to evolve the geometry to meet the physical requirements of the Lunar Zebro mission, in contrast to earlier simulations that evaluated generic flat or boxed structures.

The rover's real-world mounting requirements, the mounting region at the top, which replicates the point of contact with the lander during launch, the attachment points of the legs, and the solar panel accommodations guided the design.

To investigate structural trade-offs, three different geometries were determined and chosen:

- The baseline configuration with uniformly flat walls is represented by the cuboid.
- With its tapered width variation from bottom to top along the front and back sides, it may be possible to use less material without sacrificing stiffness.
- Lofted profile would use a continuous, smooth curvature and slope to improve stiffness naturally through form and lessen stress concentrations.

Every design was examined for how these forms interacted with modal frequencies under dynamic conditions in addition to global displacement and stress distribution under static loading. Furthermore, the emphasis was on determining which geometry carried the least weight. Beyond merely supporting external loads, the chassis had to house internal electronics, provide thermal insulation, and support other components structurally without sacrificing the lightweight objective.

To further adjust the stiffness-mass performance, a set of design parameters was added. These included stiffeners (strategically positioned ribs allowed for reduced wall thickness while maintaining stiffness) and shape (which affected load path efficiency) in which the stiffeners were attached.

5.1. Shape Modification

Lofted and tapered geometries were created to refine geometry and increase mechanical performance while attaining mass efficiency. The lofted and tapered geometries were purposefully designed to satisfy the Lunar Zebro chassis mechanical and operational requirements, not just for aesthetic or volumetric reasons.

5.1.1. Lofted Geometry: Conceptual and Mechanical Evaluation

To increase stiffness and decrease overall mass especially in the top wall, which is frequently bent by launch-induced accelerations, the lofted concept was introduced. The lofting was intended to be a sloping elevation that began at a fixed height of 45 mm above the bottom wall. The top wall area was trimmed from 200 × 140 mm to 160 × 120 mm by applying this slope consistently across the chassis on four sides. This effectively removed extra material without sacrificing functionality at the same wall thickness of 0.69 mm as the cuboid.

From a mechanical viewpoint, this decrease in surface area improved the top wall's bending stiffness while maintaining the same thickness because shorter spans are inherently better at

resisting deflection. Crucially, the top surface was left intact so that the necessary solar panel could still be installed. Further mechanical and environmental benefits were provided by the filleted edges' natural curvature, which was an intrinsic feature of the lofted profile.

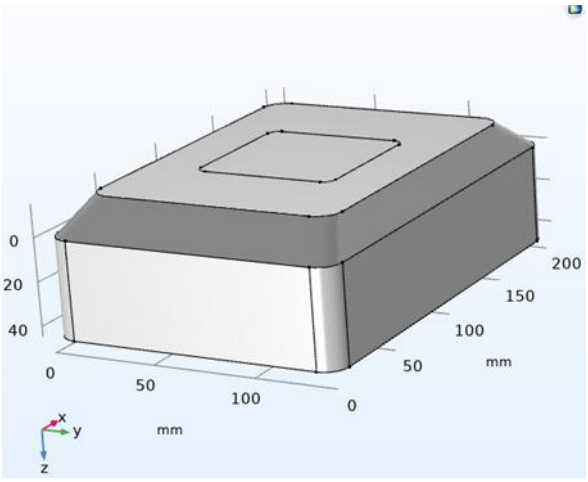

Figure 31: Lofted geometry in COMSOL

5.1.1.1. Mass Comparison and Structural Response

The chassis mass was significantly impacted by the change from a cuboid to a lofted form. The lofted configuration resulted in a weight of 98.9 g (7.44% mass reduction) from the calculated total mass of the cuboid geometry, which was 106.86 g. This decrease in material use was achieved without sacrificing structural integrity or surface continuity.

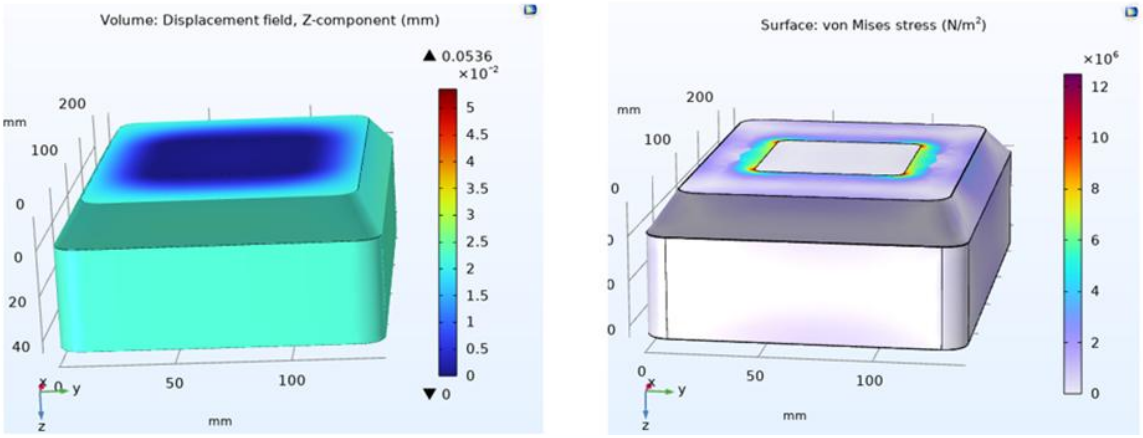

Figure 32: Displacement and stress distribution of Lofted geometry

The lofted geometry demonstrated obvious mechanical benefits beyond mass reduction. The lofted design's maximum displacement under a 10g body load in the Z-direction was 0.0536 mm, which is less than the cuboid counterpart's 0.0913 mm. This approximately 41% decrease in vertical deflection supports the mechanical principle that stiffness is increased by reducing the top wall span, particularly when wall thickness and boundary constraints are preserved. These results were corroborated by stress plots, which showed that von Mises stress was better distributed in the lofted design because of its curved form, but it remained concentrated around the mounting regions in both geometries.

5.1.1.2. Modal Performance and Center of gravity (CoG)

Using the same boundary conditions and material configuration as before, an eigenfrequency analysis was conducted on the entire lofted chassis to make sure the revised lofted geometry was not only structurally stiffer and lighter but also dynamically robust. The first natural frequency of the lofted geometry was determined to be 170.73 Hz, which greatly exceeds the minimum threshold and provides a strong dynamic safety margin. The first six natural frequencies are listed in Table 14.

Mode	Lofted geometry (Hz)
1	170.73
2	243.61
3	284.75
4	516.44
5	680.63
6	1031.7

Table 14. Eigenfrequencies of Lofted geometry

To evaluate the stability and mobility features essential for a legged rover such as the Lunar Zebro, the center of gravity (CoG) of the lofted design was computed and contrasted with the cuboid configuration. By dividing the first moment of mass about the vertical (Z) axis by the total mass, the CoG was calculated.

5.1.1.3. Analytical calculations of CoG

Cuboid	**Lofted**
$\int z \cdot \rho \cdot t$ (z moment) = 0.0032110	$\int z \cdot \rho \cdot t$ = 0.0017108
$\int \rho \cdot t$ (total mass) = 0.10687	$\int \rho \cdot t$ = 0.098981
CG_z = 0.0032110/0.10687 = 30 mm	CG_z = 0.0017108/0.098981 = 17.29 mm

As expected, given the flat top and uniform height, the center of gravity was discovered to be 30 mm above the base. The lofted chassis, on the other hand, had a substantially lower CoG of 17.29 mm because of its sloped profile and decreased mass. In the low-gravity environment of the Moon, this 12.71 mm downward shift in the center of gravity suggests improved stability.

5.1.2. Taper Geometry: Conceptual and Mechanical Evaluation

Another structural change investigated was a tapered geometry, which also aimed to improve mechanical response while using less material. The goal of the taper concept was to introduce an inclined profile along the front and back walls only, leaving the side walls vertical to maintain functional leg interfaces, in contrast to the lofted design, which involved all four walls sloping toward a smaller top surface. The top wall surface area was reduced from the original 200 × 140 mm to a narrower 160 × 140 mm by tapering only two opposing walls, all the while maintaining the sidewall geometry needed for stable leg attachment. Because the inclined profile removed some of the upper volume, this tapering mechanically saved mass. At the same time, a shorter span made the top wall more rigid, which decreased deflection under body weight. The top panel's reduced unsupported width translated into improved resistance to flexural deformation during launch loading, much like the lofted concept.

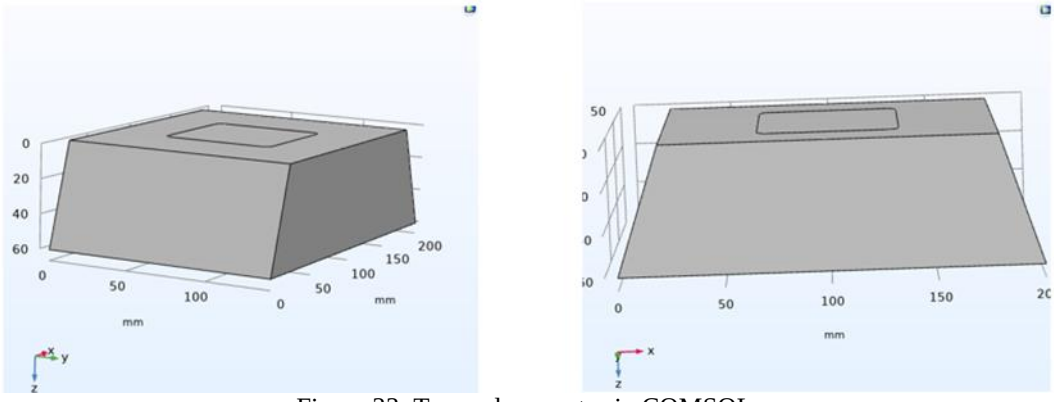

Figure 33: Tapered geometry in COMSOL

5.1.2.1. Mass Comparison and Structural Response

The 0.69 mm wall thickness stayed constant. This design change reduced the cuboid's total mass from 106.86 g to 99.03 g. Despite not being as lightweight as the lofted design (98.9 g), the tapered geometry still produced a 7.3% mass reduction when compared to the original box configuration, suggesting a good balance between material usage and geometric form.

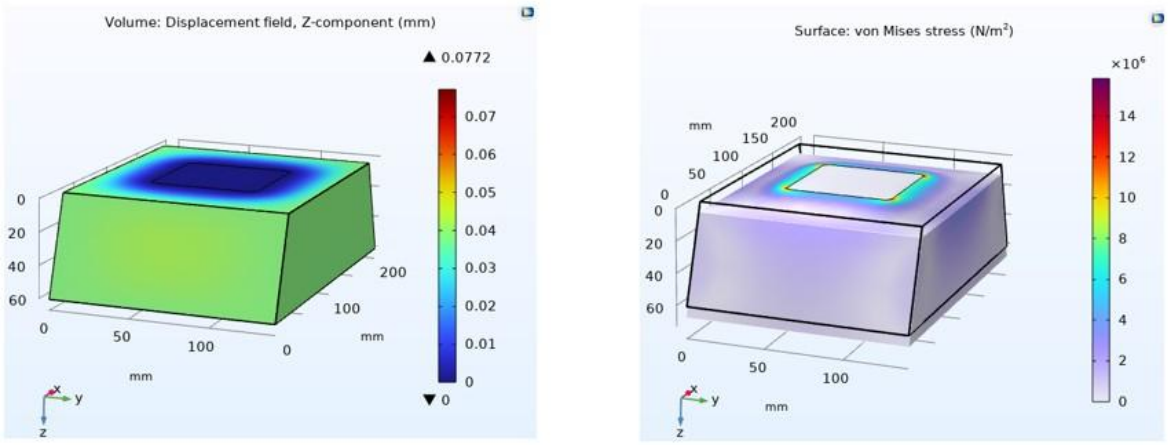

Figure 34: Displacement and stress distribution of Tapered geometry

The tapering resulted in noticeable improvements in displacement performance under body loading from a mechanical standpoint. The maximum displacement measured was 0.0772 mm, greater than the lofted geometry's 0.0536 mm but less than the cuboid's 0.0913 mm. Because of the less uniform slope and more localized load paths, tapering is marginally less effective than lofting at distributing stresses across the surface.

5.1.2.2. Modal Performance

The tapered geometry's vibrational performance under launch conditions was evaluated using an eigenfrequency analysis. It was discovered that 143.93 Hz was the first natural frequency. This result is marginally below the first mode of the lofted configuration, which is 170.73 Hz, but it is still well above the crucial 100 Hz safety threshold.

Mode	Tapered geometry (Hz)
1	143.93
2	189.45
3	230.18
4	487.51
5	677.7
6	1011.5

Table 15. Eigenfrequencies of Tapered geometry

5.1.3. Comparative analysis between Cuboid, Tapered and Lofted Geometry

The following table offers a summary of the results and a comparison of the three geometries based on eigenfrequency, mass, and displacement.

Configuration	Wall Thickness (mm)	1st Eigenfrequency (Hz)	Max Displacement (mm)	Mass and % reduction (vs Cuboid)
Cuboid (Baseline)	0.69	114.68	0.090	106.86 g
Tapered	0.69	143.93	0.0776	99.03 g (7.32% reduction)
Lofted	0.69	170.73	0.0536	98.9 g (7.44% reduction)

Table 16. Modal, displacement, and mass differences between the three geometries

Internal Volume comparison

Geometry	Total geometric volume	Wall volume	Internal Volume and % reduction compared to cuboid
Cuboid (baseline)	0.0016800 m^3	6.6792e^{-5} m^3	1613208 mm^3
Tapered	0.0015120 m^3	6.1899e^{-5} m^3	1450101 mm^3 (10.11% reduction)
Lofted	0.0016068 m^3	6.1855e^{-5} m^3	1544945 mm^3 (4.23% reduction)

Table 17. Internal Volume comparison between the three geometries

The impact of geometric modifications on usable internal space which is a crucial component for integrating onboard systems like batteries, electronics, and mechanical subassemblies was assessed by comparing the internal volume of the three configurations, cuboid, lofted, and tapered respectively. With a total external volume of 0.0016800 m^3 and a wall volume of 6.6792×10^{-5} m^3, the cuboid geometry, which served as the baseline, produced the largest internal volume of 1,613,208 mm^3. This was the standard by which later volume reductions were measured. The internal capacity of the tapered geometry decreased. Its internal volume is only 1,450,101 mm^3, which is 10.11% less than that of the cuboid reference. This loss, along with a marginally larger wall volume (6.1899×10^{-5} m^3), suggests a less usable space-efficient design that may limit the integration of important elements. The lofted geometry, on the other hand, displayed a slight decrease in internal space to 1,544,945 mm^3, or 4.23% less than the cuboid. Even with this minor decrease, the lofted chassis maintains internal functionality and structural stiffness while achieving a lower wall volume (6.1855×10^{-5} m^3) and overall reduced mass. It is a sensible and well-balanced choice because the minor space loss is balanced by the large improvements in displacement reduction and eigenfrequency performance.

5.2. Reinforcements

The CFRP cuboid box was used in the first stage to reduce mass while maintaining structural integrity, rather than the Aluminium cuboid box. The second stage used different geometries or shapes, such as a lofted one, which helped reduce mass even more while also increasing stiffness in comparison to the cuboid. Reducing the total mass while maintaining stiffness near the reference cuboid geometry (without reinforcements) may be possible by adding reinforcements as stiffeners. The third step in lowering the mass of the chassis would be to globally reduce the wall thickness from 0.69 mm, as in the first three geometries. The addition of reinforcements in the form of stiffeners was considered as a third design strategy to further improve structural efficiency after the successful mass reduction achieved by material substitution and geometric optimization.

Stiffeners are structural elements, like flanges or ribs, that are added to mechanical parts to improve their resistance to vibration, buckling, and bending without appreciably increasing mass. Stiffeners increase load-carrying capacity and decrease deflection under applied forces by locally changing the moment of inertia. They are extensively utilized in structural, automotive, and aerospace applications where stiffness and weight efficiency are crucial performance factors. [24]

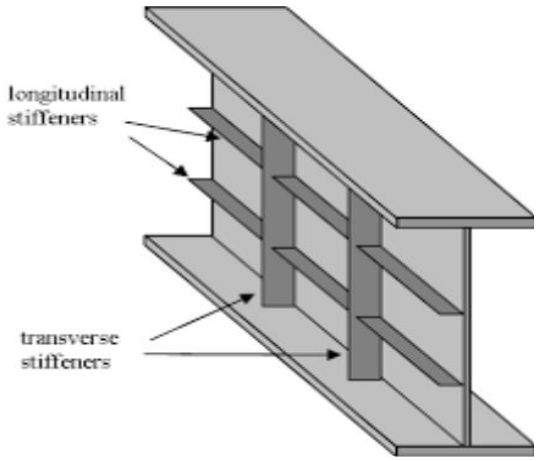

Figure 35: Rib Stiffener

A rib-reinforced cuboid geometry was created and examined to further reduce mass while preserving structural performance. Compared to the previously examined 0.69 mm configurations, the walls and stiffeners in this configuration were uniformly modelled at 0.44 mm thickness. This thickness was achieved when lowering the wall thickness from 0.69 mm till the displacement was less then or equal to baseline cuboid to maintain the stiffness. To further prevent bending and bulging under load, the cuboid's horizontal surfaces were covered with ribs that were 5 mm high and arranged in a 4-rib orthogonal pattern. Using two layers of 0.22 mm each, the CFRP layers' fiber orientation was maintained at 0 degrees, adhering to the orthotropic behaviour specified in the earlier modelling stages.

5.2.1. Static Analysis

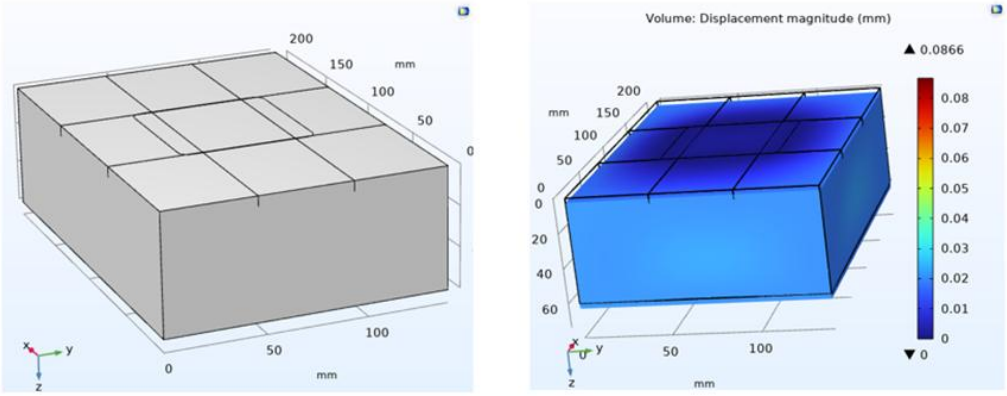

Figure 36: Static Analysis of cuboid with ribs

The structural response was still within acceptable bounds even with the thinner wall. The effectiveness of rib reinforcement was demonstrated by the maximum displacement of 0.0866 mm, which was still less than the 0.0913 mm displacement of the baseline 0.69 mm cuboid geometry. Interestingly, this performance was attained with a total mass of just 70.54 grams, which is a significant improvement over the stiffness-to-mass ratio of the original cuboid chassis, which weighed 106.86 grams.

5.2.2. Dynamic Analysis

With the first natural frequency at 230.58 Hz, the results showed a notable increase in vibrational resistance. This frequency was higher than the tapered (143.93 Hz) and even lofted (170.73 Hz) configurations, and it significantly exceeded the crucial 100 Hz launch threshold.

Mode	Cuboid geometry (Hz)
1	230.58
2	235.08
3	333.89
4	443.12
5	457.54
6	676.85

Table 18. Eigenfrequencies of cuboid with ribs

Since ribs performed better than cuboids, they were added to both the lofted and tapered geometries to test their capacity to preserve or enhance stiffness while permitting additional wall thickness reduction as shown in figure 37.

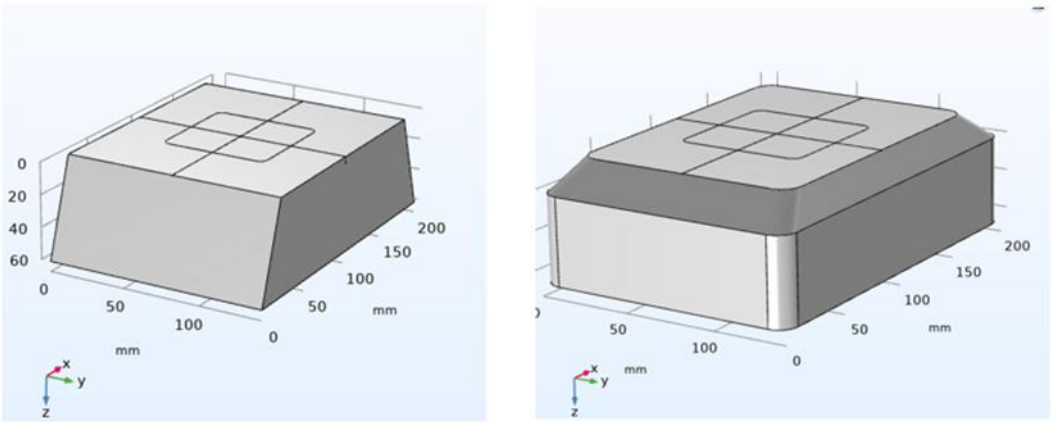

Figure 37: Tapered and Lofted geometries with ribs

To ensure consistency, tapered geometry was first tested with wall and rib thicknesses of 0.44 mm and rib heights fixed at 5 mm. However, the displacement values of the tapered configuration with ribs were higher than the acceptable threshold, even exceeding the 0.09 mm displacement of the original cuboid reference. To bring its performance within target, its wall and rib thickness were increased to 0.48 mm. To allow for a direct and equitable comparison of the two designs, the lofted geometry with ribs was also modelled with 0.48 mm thickness while keeping the rib height constant.

5.2.3. Comparison flow based on Eigenfrequency, Displacement and Mass

The three configurations cuboid, tapered and lofted were compared based on the same wall thickness in which lofted outperformed the others. When adding ribs, the mass was decreased by decreasing the wall thickness while maintaining the displacement baseline regarding cuboid displacement. While tapered ribbed required two ribs to achieve the displacement but at a higher wall thickness, the overall mass was still less than that of cuboid. In contrast, cuboid ribbed required four ribs to achieve the displacement and specific wall thickness. Because the original wall thickness (0.44 mm) with two ribs in the tapered ribbed geometry was causing more displacement than baseline, the higher wall thickness was calculated. In the end, lofted ribbed and tapered ribbed were compared with the same wall thickness and number of ribs. Lofted ribbed provided a lower displacement, a lower mass, and a comparable first eigenfrequency. Lofted ribbed thus performed better than the other configurations. The table below displays the results.

Configuration	Wall Thickness (mm)	No. of Ribs	1st Eigenfrequency (Hz)	Max Displacement (mm)	Mass and % Reduction (vs Cuboid)
Cuboid (Baseline)	0.69	0	114.68	0.09	106.86 g
Lofted Ribbed	**0.48**	**2**	**200.30**	**0.0772**	**69.92 g (34.56% reduction)**
Tapered Ribbed	0.48	2	200.81	0.0835	70.048 g (34.44% reduction)
Tapered Ribbed	0.44	2	196.26	0.0948	64.21 g (39.91% reduction)
Cuboid Ribbed	0.44	4	230.58	0.0866	70.54 g (33.98% reduction)
Cuboid Ribbed	0.44	2	155.58	0.104	69.34 g (35.11% reduction)

Table 19. Comparison flow of all ribbed geometries

Quantitative Assessment and Final Selection

To maximize the CFRP-based Lunar Zebro chassis mechanical performance under body load conditions that mimic launch acceleration, several configurations were assessed. The maximum displacement, first eigenfrequency, and structural mass of each design were evaluated, with a focus on enhancing vibrational resistance and mass reduction without sacrificing structural integrity.

The baseline cuboid shape, which had no ribs and walls that were 0.69 mm thick, had the lowest first eigenfrequency (114.68 Hz) and the highest mass (106.86 g), just above the 100 Hz minimum safety threshold. Despite being structurally stable, it was the least desirable choice because of its largest displacement under loading (0.09 mm). The lofted and tapered geometries with consistent wall thickness (0.69 mm) showed significant improvements. Specifically, the lofted box achieved a significantly higher eigenfrequency of 170.73 Hz and an exceptionally low displacement of 0.0536 mm, the lowest of all tested designs. The natural geometric stiffening that inclined side walls provide is responsible for these advantages. But compared to the cuboid, this only resulted in a slight mass loss (7.44%).

Stiffness enhancement gained a new dimension with rib reinforcement. Despite having four internal ribs and a thinner 0.44 mm wall, the ribbed flat cuboid produced the highest eigenfrequency (230.58 Hz) and a respectable mass savings (33.98%). Its displacement was still high (0.0866 mm), though, and the increased number of ribs might make internal space management and manufacturing more difficult. The designs with two ribs and a reduced 0.48 mm wall thickness that were tapered and lofted ribbed showed the most promising results. Both structural efficiency and useful mass reduction were attained by these configurations. The tapered ribbed structure demonstrated a 34.44% mass reduction while preserving safe displacement (0.0835 mm) and achieved an eigenfrequency of 200.81 Hz. While still exceeding 200 Hz in eigenfrequency, the lofted ribbed design provided a slightly better displacement (0.0772 mm) and a 34.56% mass reduction. These findings show that superior performance across all important parameters can be attained by combining geometric shaping with incorporation of ribs.

In conclusion, for this mission profile that incorporates CFRP material, the lofted ribbed configuration (0.48 mm walls, 2 ribs) performs better than any other. With a low displacement (0.0772 mm) and a safe eigenfrequency above 200 Hz, it achieves high stiffness structurally. In practical terms, it provides the largest mass reduction (nearly 35%) with a rib layout when compared to the reference cuboid without ribs. It is the most effective and mission-ready chassis design because it creatively blends geometric stiffening with minimal reinforcement to provide maximum performance with the least amount of material. Refer to the appendix for lofted geometry dimensional measurements.

5.2.4. Tsai-Wu Criterion to Validate Failure Index

For every tested geometry, the Tsai-Wu failure index was calculated to confirm that the ribbed configurations retained safety margins under high loading. As previously mentioned, values below 1.0 indicate structural integrity across all plies, making this scalar index a reliable indicator of failure risk under multi-axial stress.

Configuration	Wall Thickness (mm)	No. of Ribs	Tsai-Wu
Lofted Ribbed	**0.48**	**2**	**0.147**
Tapered Ribbed	0.48	2	0.161
Ribbed (Flat Cuboid)	0.44	4	0.212
Lofted	0.69	0	0.228
Tapered	0.69	0	0.289
Cuboid (Baseline)	0.69	0	0.411

Table 20. Tsai-Wu index of the different configurations

With the lowest Tsai-Wu index of 0.147 in the entire design matrix, the Lofted Ribbed geometry was the best-performing configuration overall. It shows that in addition to providing

the best performance in terms of displacement, mass, and eigenfrequency, the design offers the largest margin against composite ply failure under body load and launch-induced stresses.

5.2.5. Reduction of wall thickness of Lofted ribbed geometry

The maximum displacement of 0.0772 mm was attained by the lofted ribbed geometry with two ribs and a wall thickness of 0.48 mm. This is less than the baseline cuboid displacement of 0.090 mm. In addition to attaining a 34.56% mass reduction and a markedly enhanced first eigenfrequency of 200.30 Hz, this verified a distinct margin in displacement performance. To maximize structural efficiency, this margin gave confidence to investigate additional mass reduction by gradually lowering the wall thickness until the displacement got close to the baseline reference. The lofted ribbed configuration maintained its superior stiffness-to-mass performance throughout this iterative process.

Configuration	Wall Thickness (mm)	No. of Ribs	1st Eigenfrequency (Hz)	Max Displacement (mm)	Mass and Difference (vs Cuboid)
Lofted Ribbed	0.435	2	194.87	0.0894	63.36 g (40.70% reduction)
Cuboid (Baseline)	0.69	0	114.68	0.090	106.86 g

Table 21. Wall thickness reduction and evaluation of Displacement, mass and eigenfrequency

Utilizing the available displacement margin in comparison to the cuboid baseline, the wall thickness of the lofted ribbed geometry was decreased to 0.435 mm. The maximum displacement stayed at 0.0894 mm, which was nearly equal to the cuboid's 0.09 mm, but the mass was decreased to 63.36 g (40.7% reduction) from the original cuboid design. The first eigenfrequency also remained high at 194.87 Hz to maintain dynamic stability.

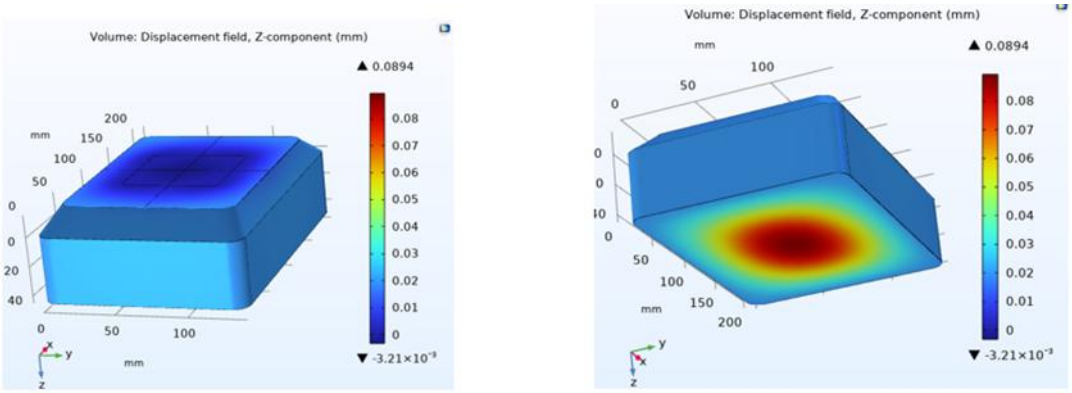

Figure 38: Displacement plot of Lofted geometry with 2 ribs with wall and rib thickness being 0.435 mm

5.2.6. Orientation of the Lofted ribbed geometry

Under vertical body load, the displacement response of the lofted ribbed geometry was further investigated in various orientations, with the results displayed in the figure.

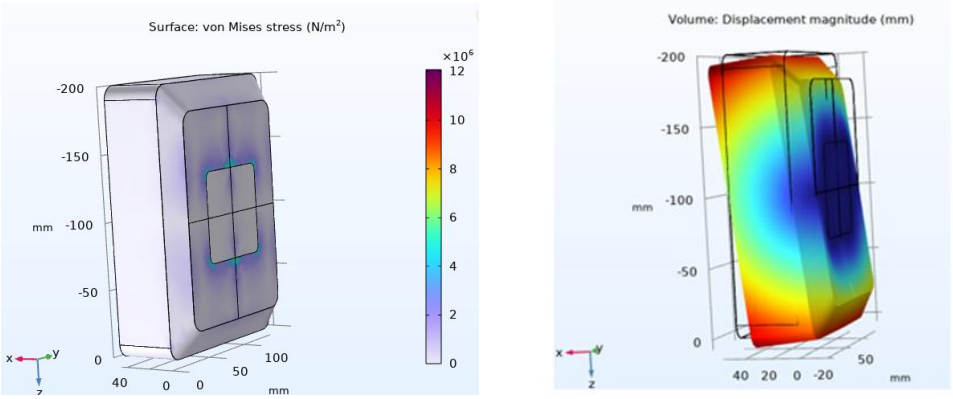

Figure 39. Stress plot and Displacement Magnitude plot of Orientation 2 of the Lofted chassis

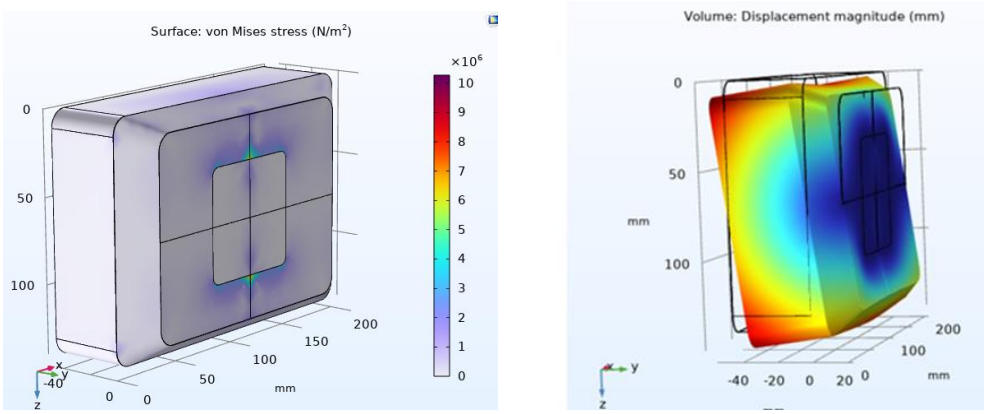

Figure 40: Stress plot and Displacement magnitude plot of Orientation 3 of the Lofted chassis

As compared to Orientation 1 (0.0894 mm), Orientations 2 and 3 displayed lower displacement values (0.0228 mm and 0.0176 mm, respectively); however, these smaller displacements were concentrated precisely in areas where the rover's legs would be mounted. By showing this displacement away from leg-attachment regions, despite having a higher overall displacement, Orientation 1 maintained integrity where structural support is most important and was chosen as the best configuration, to balance performance and functional requirements.

In every tested orientation, the lofted ribbed chassis, which has a thickness of 0.435 mm, consistently displayed lower displacement values than the baseline cuboid, which has a thickness of 0.69 mm as demonstrated in table 25. This decrease can be explained by the additional reinforcement provided by the ribs and the natural stiffness of the curved lofted walls, which work together to prevent local bending and more evenly distribute loads.

Orientation	**Displacement in mm (Cuboid)**	**Displacement in mm (Lofted with ribs)**
Orientation 1	0.09	0.0894
Orientation 2	0.0593	0.0228
Orientation 3	0.0361	0.0176

Table 22. Displacement of Lofted Ribbed geometry compared to Cuboid in different chassis orientations

5.3. Geometric Stiffeners

Building on the notable mass reduction that was accomplished by reducing the wall thickness from 0.48 mm to 0.435 mm, it was realized that there was a chance to increase the chassis stiffness even more with a negligible mass penalty. Geometric features could be incorporated into thin-walled structures to improve their resistance to bending and bulging under load, taking inspiration from vacuum-formed plastic products, sheet metal design techniques, and the structural principles found in airplane wings.

Trays, embossed containers, corrugated sheets, and ordinary plastic bottles were used as examples, as shown in Figure 41, show how precisely positioned embossed patterns, grooves, and curvatures greatly increased stiffness in thin sections. [25]

Geometric stiffeners were thought to be added to locally increase stiffness by raising the moment of inertia, and decrease displacement without significantly increasing the amount of material usage. This idea was investigated for possible use in the nano rover chassis, specifically in the spaces between the legs where side walls tended to bulge as a result of body loads and applied boundary conditions. It was thought that both localized and global stiffness could be increased by employing such geometric improvements. Thus, much of the mass efficiency already attained through thickness reduction may be preserved while the chassis stiffness and displacement are improved.

Figure 41: Sheet metal design, Vacuum formed products and Aeroplane Wing panel depicting the geometric features

5.3.1. Geometric Stiffener Concepts

To increase the chassis walls' stiffness while minimizing extra mass, four potential feature concepts were created. These ideas included an emboss pattern, a rectangular cell structure, a series of dimples and a curved emboss design.

In Figure 42, the figures on the right show enlarged side wall features for clarity, while the figures on the left display the overall lofted chassis geometry (up to 45 mm from the bottom) for context. AutoCAD and COMSOL software was used to create these designs, guaranteeing accuracy and CAD-CAM workflow compatibility. The purpose of each of these geometric elements was to mitigate local bending and side wall bulging, placed especially in the spaces between the rover legs. These concepts prepared the way for the subsequent simulation and assessment stage, which would measure how well they reduced displacement and enhanced global stiffness.

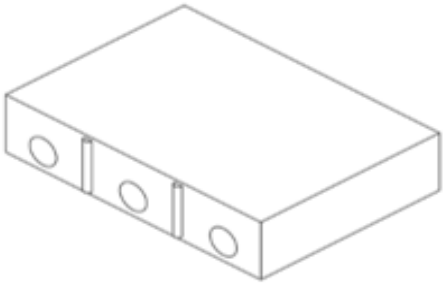

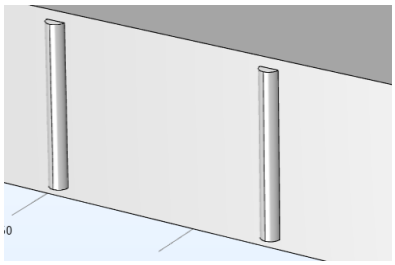

Emboss

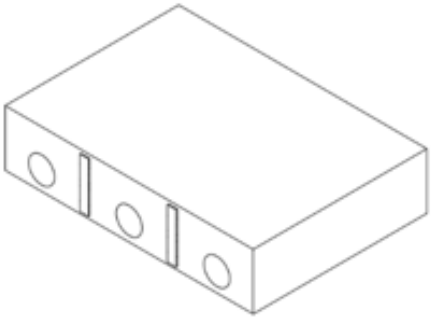

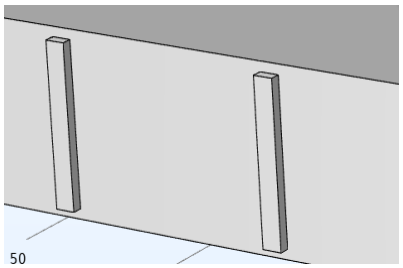

Rectangular Cell

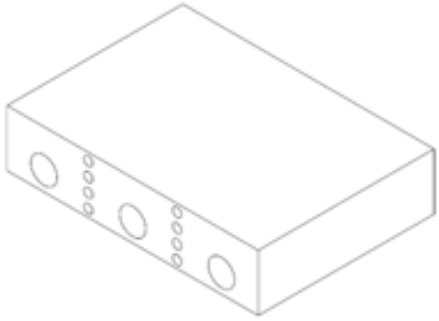

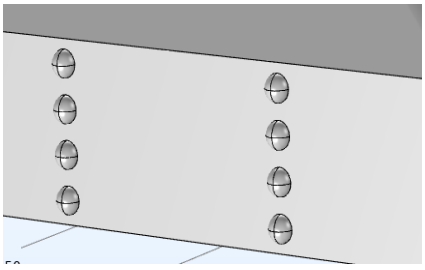

Dimple

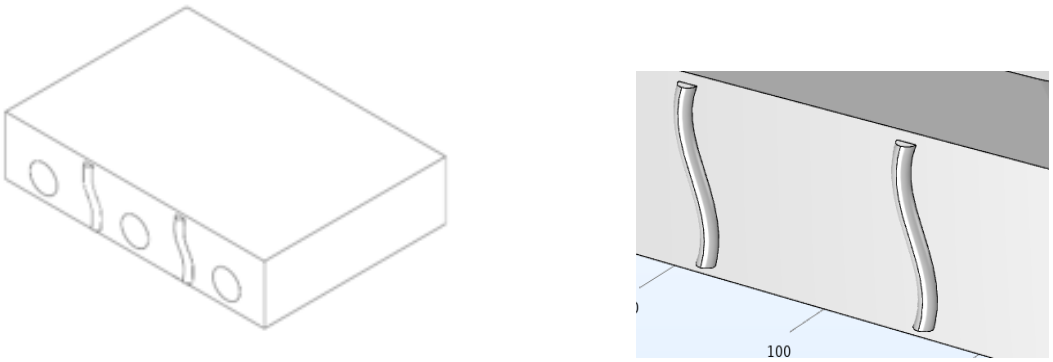

Curved Emboss

Figure 42: Different geometric features made in AutoCAD and COMSOL

The dimensions and extrusion parameters for the geometric reinforcement features were meticulously established to guarantee a smooth integration within the chassis available side wall spaces. The vertical arrangement of dimples (hemi-spherical features), as seen in Figure 43, was situated on the side wall of the chassis (till 45 mm from bottom) and had an overall feature length of 40 mm. Each dimple's diameter was set at 7 mm, with top and bottom clearances of 2.5 mm to prevent interference with other faces.

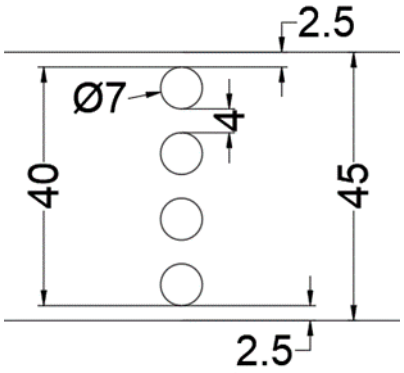

Figure 43: Dimensions of the Dimple features (All dimensions are in mm)

The other three feature types, emboss, rectangular cells, and curved emboss were subject to comparable spatial restrictions and a total length of 40 mm. The rectangular cell's width was 6 mm, as was the diameter of the half-cylindrical emboss and curved emboss. To ensure adequate stiffening effect while preserving compactness, the maximum extrusion distances (extension from the side wall surface) were set at 3 mm for the emboss, modular cell, and curved emboss designs, and 3.5 mm for the dimple pattern. After considering the distances between the legs and ensuring that any extrusions would not impede leg movement or conflict with external mounting requirements, these parameters were selected. By using this method, the designs maximized the potential for structural reinforcement while adhering to functional constraints.

5.3.2. Implementation of Rectangular cell feature

A rectangular cell geometric feature was added to the outer side walls of the optimized lofted ribbed chassis to improve its mechanical performance even more. The lofted ribbed geometry with two internal ribs and a wall thickness of 0.435 mm was chosen for evaluation because it had previously shown a good balance between mass and displacement, as shown in Figure 44.

Rectangular cell extrusions were added to the side walls' exterior surfaces in the revised design, staying within the 45 mm height limit and adhering to the previously established dimensional constraints.

When the body load was applied, the von Mises stress and displacement plots demonstrated how well the feature worked to redistribute stress and marginally suppress deformation, particularly in the side regions where bulging had previously been seen.

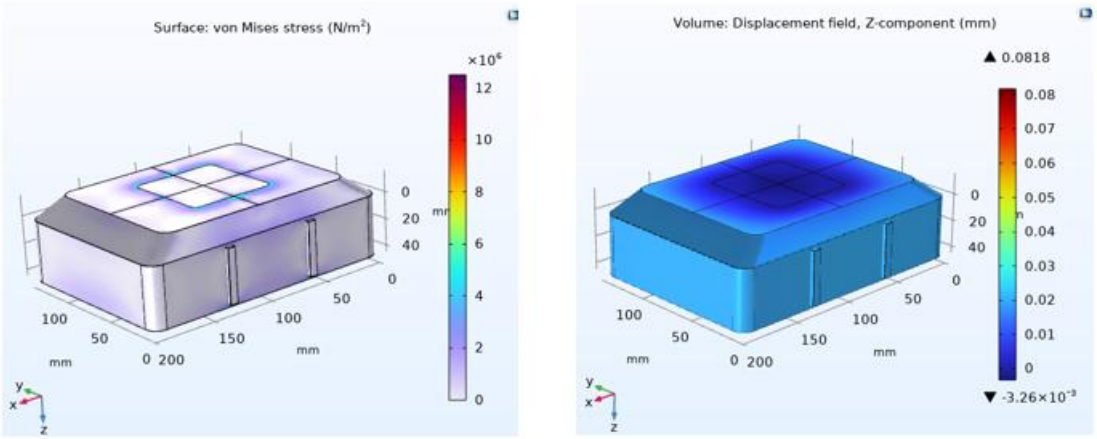

Figure 44: Stress distribution and displacement plot for the lofted geometry with ribs integrating rectangular cell feature

Between the modified version with rectangular cells and the baseline lofted ribbed geometry, a comparative analysis was carried out. Based on the data in the performance table, it was clear that adding the feature reduced the maximum displacement from 0.0894 mm to 0.0818 mm (8.5% reduction) while keeping the mass at a similar level, from 63.36 g to 64.13 g (only 1.2% increase). The structural stiffness was maintained, as evidenced by the slight drop in eigenfrequency from 194.87 Hz to 193.83 Hz.

Configuration	Wall Thickness (mm)	No. of Ribs	1st Eigenfrequency (Hz)	Max Displacement (mm)	Mass and Difference (vs Cuboid)
Lofted Ribbed (without feature)	0.435	2	194.87	0.0894	63.36 g
Lofted Ribbed (with cell)	0.435	2	193.83	0.0818	64.13 g

Table 23. Comparative analysis between the Lofted ribbed configuration without feature vs with rectangular cell feature

It supported the idea that thin-walled composite enclosures can benefit from geometric alterations motivated by forming techniques and other approaches. As a result, every geometric feature that is visible in the figure was assessed under the specified boundary conditions.

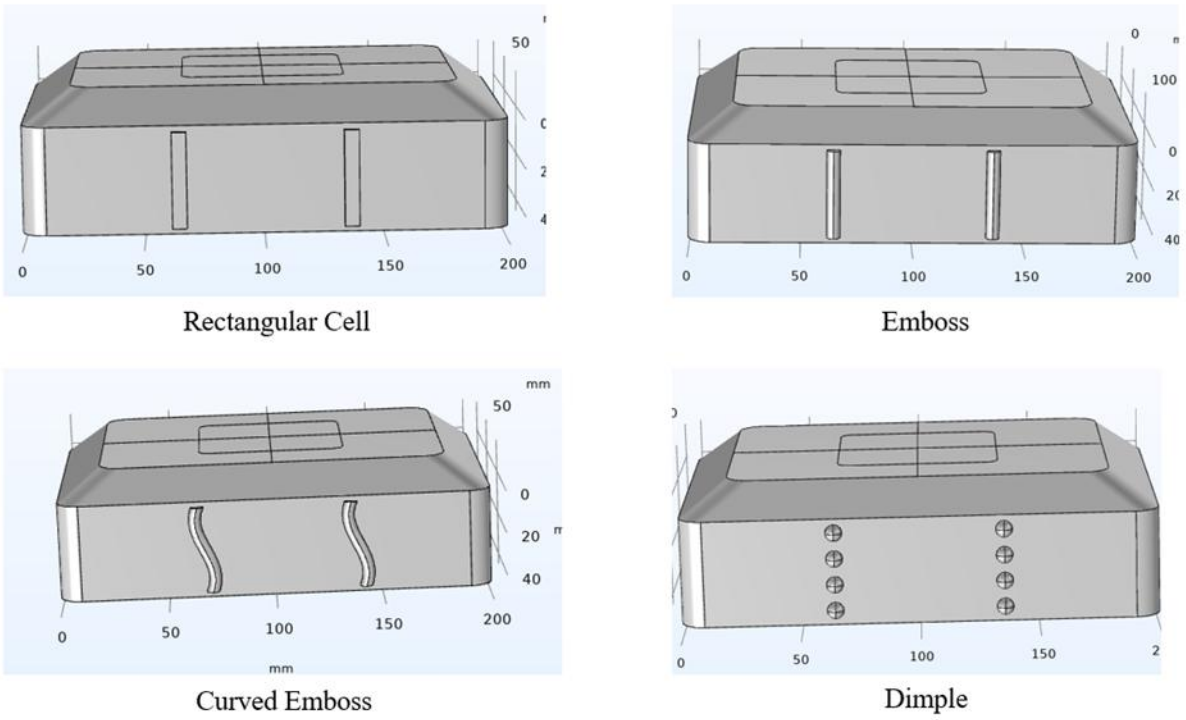

Figure 45: Different geometries involving geometric stiffeners in COMSOL

5.3.3. Comparative analysis between different stiffening features

A thorough evaluation was conducted by embedding four different stiffening features onto the side walls of the optimized lofted ribbed geometry with 0.435 mm wall thickness and two internal ribs, as shown in the table, to compare the performance of different geometric reinforcement strategies.

Features	1st Eigenfrequency (Hz)	Max Displacement (mm) and Reduction (wrt without feature)	Mass and Gain (wrt without feature)
Rectangular Cell	**193.83**	**0.0818 (8.5% reduction)**	**64.13 g (1.2% gain)**
Emboss	195	0.0822 (8.05% reduction)	63.81 g (0.7% gain)
Curved emboss	194.99	0.0833 (6.82% reduction)	63.85 g (0.76% gain)
Dimple	195.63	0.0858 (4.02% reduction)	63.77 g (0.64% gain)
Without Feature	194.87	0.0894	63.36 g

Table 24. Comparative analysis of different features based on eigenfrequency, displacement and mass

With a maximum Z-displacement of 0.0818 mm, an 8.5% decrease from the unfeatured baseline, the Rectangular Cell design demonstrated the best displacement reduction. This improvement was the most effective in increasing stiffness, which was the main objective here, and it came with a slight 1.2% mass increase.

Following closely behind, the Straight Emboss and Curved Emboss features demonstrated displacement reductions of 8.05% and 6.82%, respectively. These designs showed a slightly stiffer dynamic response, as evidenced by slightly higher eigenfrequencies than the baseline. Despite having the highest eigenfrequency (195.63 Hz), the dimple pattern only reduced displacement by 4.02%, indicating that while it increases vibrational stiffness, its impact on global bending stiffness is minimal.

The Rectangular Cell was the most advantageous option overall due to its displacement performance and stress redistribution benefit, even though it resulted in a very slight decrease in eigenfrequency.

5.3.4. The Final design of the Chassis

The chassis profile in the final configuration, shown in Figure 46, was made entirely of Carbon Fiber Reinforced Polymer (CFRP).

By eliminating extra volume near the top, the lofted geometry helped reduce mass while providing better global stiffness compared to its flat-walled counterparts.

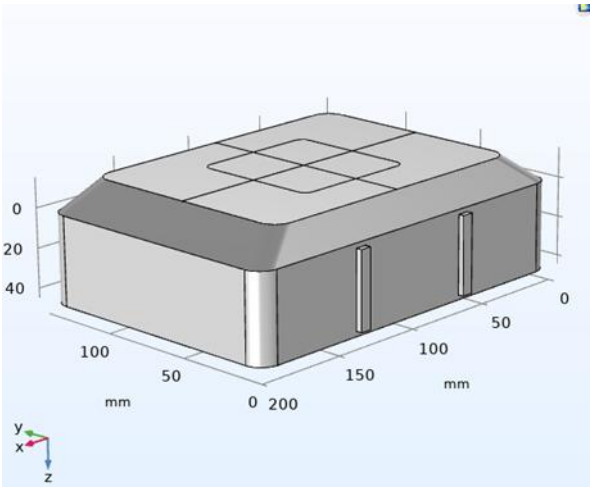

Figure 46: Final chassis design incorporating CFRP material, Lofted geometry, ribs and rectangular cell features

Two orthogonal ribs were embedded internally along the top wall to further improve structural integrity, especially under compressive and bending stresses on the top surface. These ribs effectively suppressed vibration modes, improved load-carrying capacity, and greatly reduced mass while maintaining displacements within allowable bounds.

Ultimately, the rectangular cell stiffener was selected as the optimal feature for the side wall because it provided a well-balanced combination of geometric simplicity and mechanical effectiveness. The rectangular cell, which served as an external vertical reinforcement, increased resistance against out-of-plane deformations, especially in the mid-region of the side wall, which is prone to bulging under applied body loads because of boundary constraints.

6. Conclusion

The purpose of this thesis was to investigate whether the structural optimization of the Lunar Zebro rover chassis could be significantly aided using Carbon Fiber Reinforced Polymer (CFRP) in conjunction with design improvements and finite element modelling. The study was driven by the strict mass and launch survivability requirements that small-scale planetary rovers must meet as well as the possibility that in contrast to the traditional metallic materials, CFRP could provide better stiffness-to-weight properties.

Instead of just switching one material for another, the study sought to determine how CFRP's special qualities, particularly its anisotropy and changeable layups could be used in a methodical and mechanically sound manner. The work advanced from plate-level analysis to complete chassis models using a simulation-driven methodology that included both laminate-level optimization and geometric design changes. These actions were done to assess the material's structural behaviour as well as to develop a comprehensive understanding of how within the practical rover chassis framework, CFRP could be incorporated. The results indicate that CFRP can achieve significant mass reductions while preserving sufficient structural and dynamic performance when applied carefully with the right stacking sequences and geometrical support. Designs that performed well in simulations under launch-like conditions were made possible using symmetric cross-ply layups and ply thickness optimization. At full chassis level, the curved profiles and localized stiffening features increased the strength while reducing the mass.

From a more general standpoint, this work makes a gradual contribution to the knowledge that for space robotics, form-driven design techniques and composite materials can help create strong, lightweight structures. The application of COMSOL's Solid Mechanics and Layered Shell interfaces to resolve ply-level stresses, eigenfrequency behaviour, and failure indices in thin-walled CFRP systems shows how it supports analysis.

Geometric interventions to increase local and global stiffness were also investigated in the study. Among these, internal rib reinforcements were demonstrated to lower mass globally through reduced wall thickness, greatly reduce displacement, and increase modal safety without imposing significant mass penalties. Furthermore, sidewall extrusions and rectangular cell features were geometric stiffeners that showed quantifiable structural advantages inspired by vacuum-formed, automotive, and aerospace products. Improved directional stiffness was provided by these characteristics, particularly in CFRP thin walls. The final configuration achieved a well-balanced design with minimized mass, reduced displacement, and enhanced eigenfrequency performance which integrated both ribbed reinforcement and geometric surface stiffening.

This study reduces the mass in four stages, first by implementing CFRP instead of Aluminium on the chassis level (72% weight reduction overall), then by change in shape of cuboid design to lofted geometry (7.44% reduction compared to cuboid reference), thirdly by incorporation of ribs (34.56% reduction compared to cuboid) and lastly wall thickness reduction of the lofted ribbed geometry (40.70% reduction compared to cuboid). The geometric stiffeners on the other hand increased the stiffness by reducing the displacement by 8.5% and having a mass penalty of just 1.2%. The overall mass reduction compared to Aluminum chassis was 83.29%. Therefore, study aims to advance our understanding of how CFRP and design changes improve the structural performance of a compact lunar rover chassis.The findings offer an approach that

may be built upon and refined through further simulation, experimental validation, and manufacturing insight. It is hoped that the approaches and insights developed here will serve as a useful reference for future efforts aiming to design lightweight, efficient, and structurally reliable systems for space exploration rovers such as the Lunar Zebro. The study confirms that the incorporation of CFRP, in conjunction with advanced FEA-based geometric and structural redesign (lofted design, ribs and rectangular cell extrusions), significantly enhances both mass efficiency (83.29% reduction compared to Aluminium chassis) and structural performance of the Lunar Zebro chassis.

7. Recommendations for Future Work

The establishment of a computational framework for the structural optimization of the Lunar Zebro chassis utilizing CFRP now give rise to a few avenues to enhance the findings. Simulation models may also incorporate intricate interactions demonstrated by real-world phenomena such as thermal cycling and micrometeor impact, especially under multiphysics settings. The next step forward is to conduct experimental validation by scaled physical testing of the proposed chassis designs to verify stiffness, failure thresholds, and vibrational characteristics under conditions representative of launch and lunar operations.

Future study should explicitly use coupled thermal-mechanical models to more accurately depict the temperature extremes and gradients present on the lunar surface. Modelling the consequences of micrometeoroid impacts is also pragmatic for assessing the damage tolerance of the CFRP structure.

The correlation between the chassis and internal payload components, including the legs and control systems, merits further examination. The further approach could account for localized stress concentrations resulting from mounting interfaces and dynamic leg forces during locomotion. Additionally, the adhesive connections and interfaces between chassis components are crucial for load transmission and assembly. To improve the manufacturability and structural integrity, comprehensive analysis of joint design, interfacial tensions, and fabrication tolerances could be performed.

The proposed geometric stiffeners and curved designs must be assessed for manufacturability to guarantee practical viability, particularly when utilizing vacuum-assisted techniques or resin transfer molding.

In conclusion, while this study lays the groundwork for CFRP-based lightweight chassis design, a synthesis of further advanced modelling, experimental validation, and design-for-manufacturing research will be essential to transform these concepts into operational, space-qualified systems.

8. Appendix

Eigenfrequency Analysis on the box at 40 x 40 constraint

Mode	CFRP 0.69 mm (Hz)	CFRP 1 mm (Hz)
1	65.855	93.985
2	95.343	135.87
3	133.08	190.19
4	437	624.53
5	653.19	931.42
6	979	1393.7

Eigenfrequency Analysis on the box at 68 x 68 constraint

Mode	CFRP 0.69 mm (Hz)
1	114.68
2	182.23
3	209.26
4	469.61
5	661.19
6	1002.6

CFRP Plate Mode shapes at 0.69 mm thickness

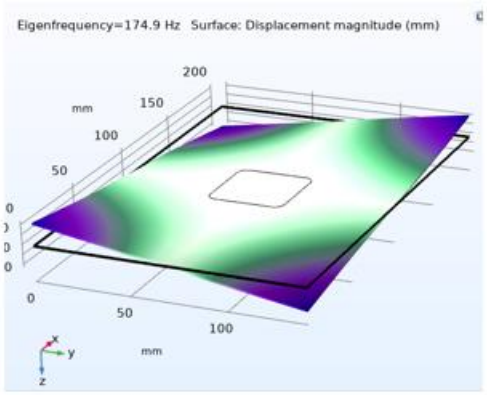

174.9 Hz

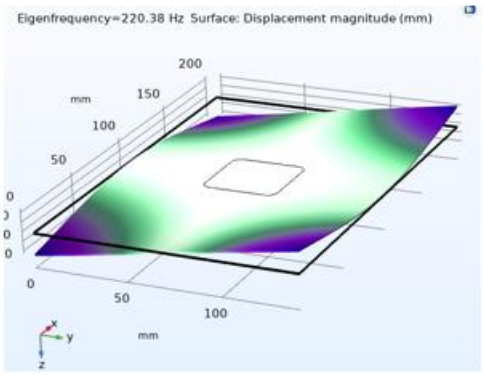

220.38 Hz

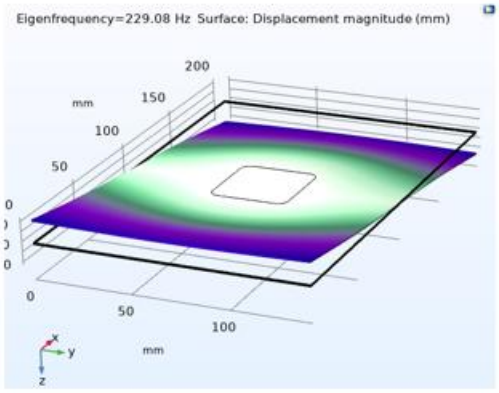

229.08 Hz

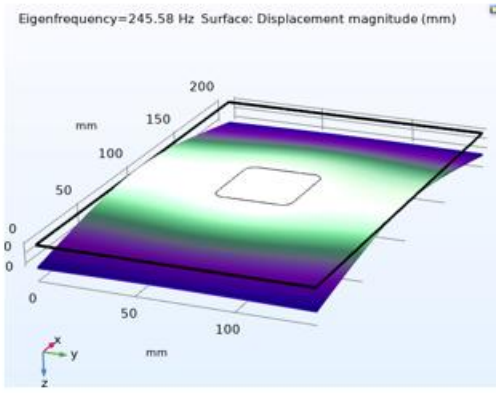

245.58 Hz

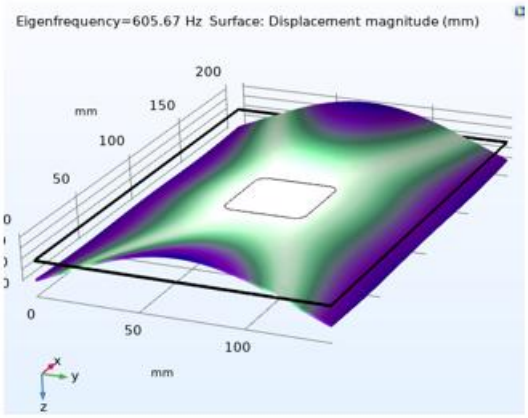

605.67 Hz

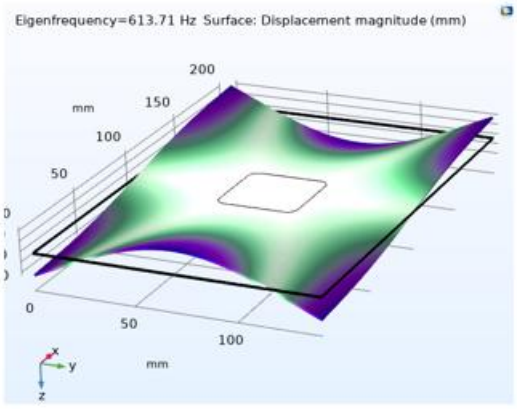

613.71 Hz

CFRP Cuboid Box Mode shapes with 68 x 68 mm square constraint

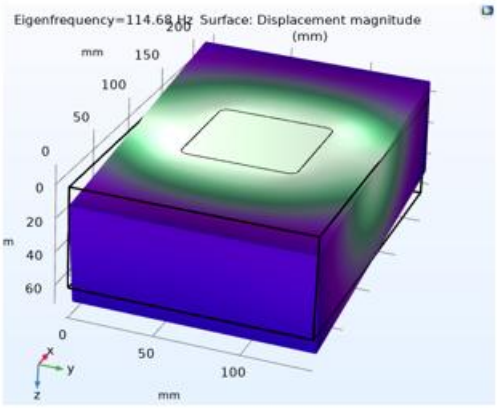

114.68 Hz

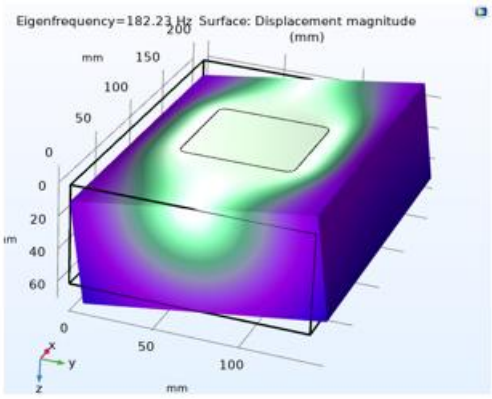

182.23Hz

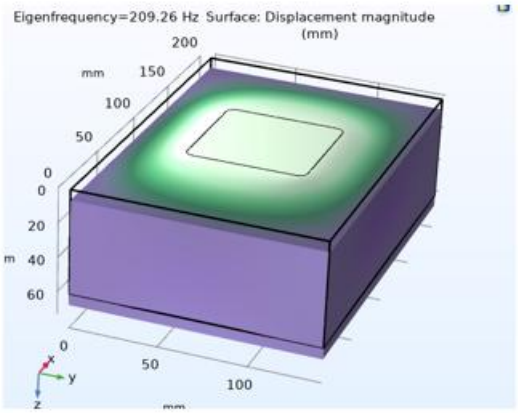

209.26 Hz

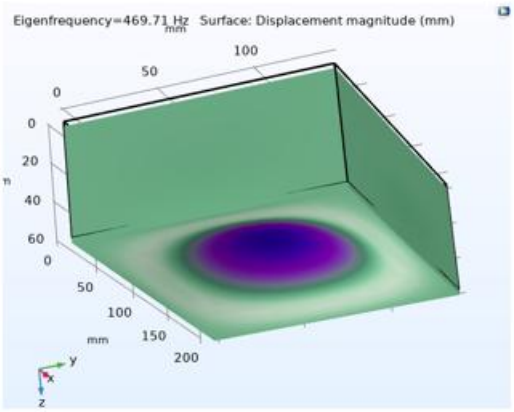

469.61 Hz

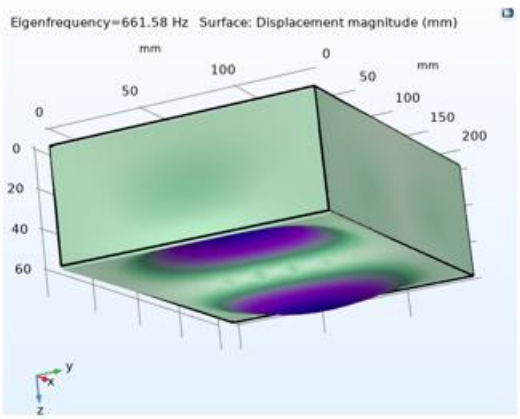

661.19 Hz

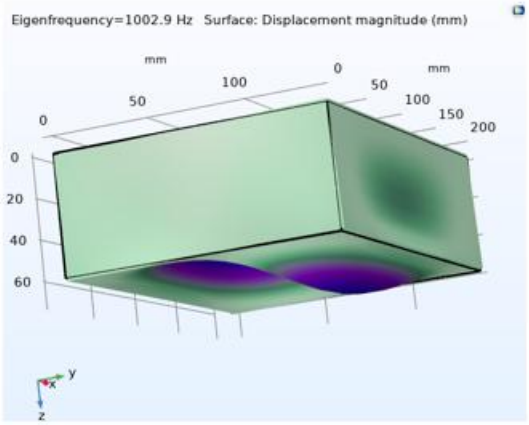

1002.6 Hz

Dimensions of Lofted Geometry

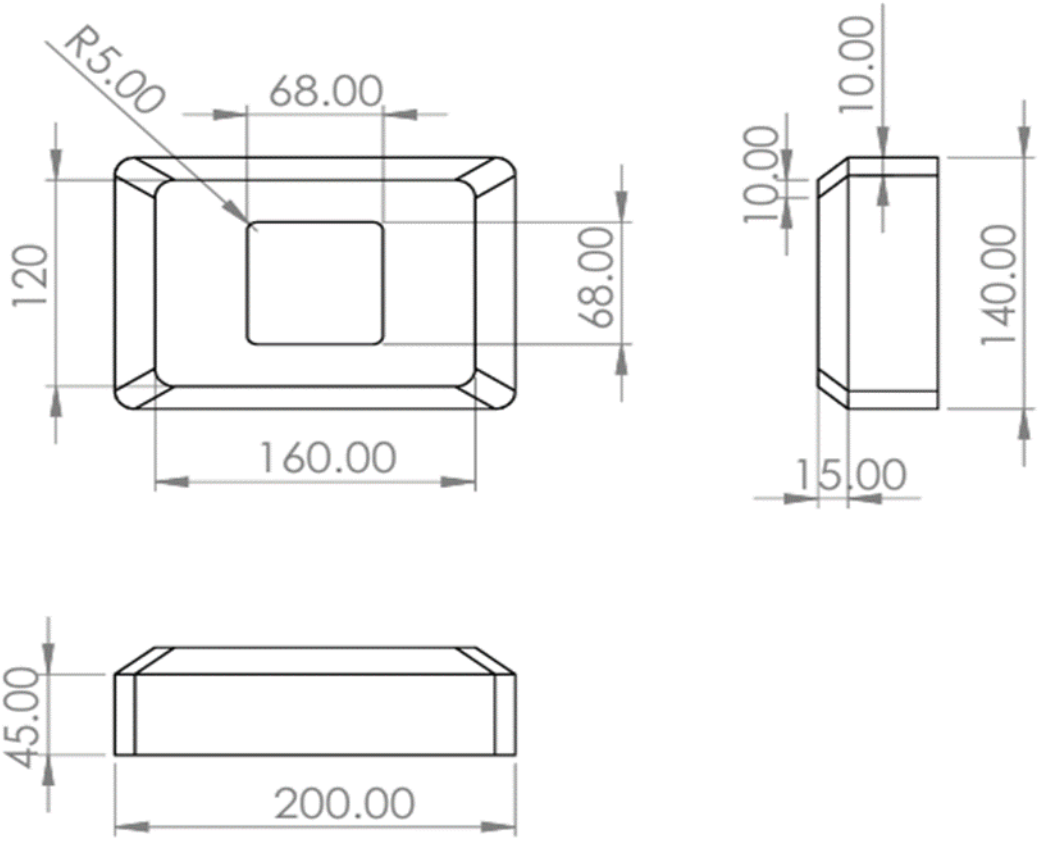

All Dimensions are in mm

Bibliography

[1] R. F. Gibson, Principles of Composite Materials, Fourth Edition, 2016.

[2] M. F. Ashby, “Technology of the 1990s: Advanced materials and predictive design.,” *Philosophical Transactions of the Royal Society of London,* vol. A322, p. 393–407, 1987.

[3] A. Bunsell, Handbook of Tensile Properties of Textile and Technical Fibers, Cambridge: Woodhead Publishing Limited, 2009.

[4] S. A. Mirdehghan, “Fibrous polymeric composites”.

[5] R. Y. G. &. S. C. T. &. D. A. Pandey, “Structural Analysis of Automotive Chassis, Design Modification,” *International Journal of Applied Engineering Research,* vol. vol. 13, pp. 9887-9892, 2018.

[6] “testbook,” 3 October 2023. [Online]. Available: https://testbook.com/mechanical-engineering/types-of-chassis.

[7] “Lunar Roving Vehicle,” 11 December 2024. [Online]. Available: https://en.wikipedia.org/wiki/Lunar_Roving_Vehicle.) .

[8] 22 November 2024. [Online]. Available: https://en.wikipedia.org/wiki/Sojourner_(rover).).

[9] .. S. T. K. .. A. S. a. C. H. A. S. V. Unnikrishnan, “Design and Development of an Intelligent Rover for Mars”.

[10] “ "Nasa,"," 19 October 2020. [Online]. Available: https://www.nasa.gov/centers-and-facilities/jpl/nasas-perseverance-rover-bringing-3d-printed-metal-parts-to-mars/.).

[11] C. S.-J. &. P. Y.-J. S. G.-H., “Rib Design for Improving the Local Stiffness of Gearbox Housing for Agricultural Electric Vehicles,” no. Modelling, Simulation and Data Analysis in Acoustical Problems II), 2019.

[12] T. H. G. Megson, Aircraft Structures for Engineering Students, 2016.

[13] W. G. G. L. Jin Nie, “Buckling Characteristics of Different Cross-Sectioned LGFR-PP Stiffeners under Axial Compression,” 2023.

[14] V. Raja, K. Venkatesan, R. Murugesan and R. K. Gnanasekaran, “Optimization of Orientation of Carbon Fiber Reinforced Polymer Based on Structural Analysis,” *International Journal of Scientific & Technology Research,* 2019.

[15] “Failure Prediction in a Laminated Composite Shell,” [Online]. Available: https://www.comsol.com/model/failure-prediction-in-a-laminated-composite-shell-65641.

[16] Q. T. Nguyen, “ Finite Element Analysis in Automobile Chassis Design.,” *Applied Mechanics and Materials. ,* pp. 461-468, 2019.

[17] “Aluminium,” [Online]. Available: https://en.wikipedia.org/wiki/Aluminium#:~:text=,.

[18] R. K. Joki, “Cohesive zone model for mode I and mode II,” *DACOMAT,* 2019.

[19] M. &. C. M. A. Alfano, “"Finite element interface models for the delamination analysis of laminated composites: mechanical and computational issues.",” *International Journal for Numerical Methods in Engineering,* p. 1701–1736, 2001.

[20] “Tsai–Wu failure criterion for orthotropic materials,” [Online]. Available: https://en.wikipedia.org/wiki/Tsai%E2%80%93Wu_failure_criterion#Tsai%E2%80%93Wu_failure_criterion_for_orthotropic_materials.

[21] N. L. Kumari, A. Mehar, M. Abdulrahman, S. Tatineni , E. . V. Shashank and J. T. Muthyala, “Performance Analysis of Ply Orientation in Composite Laminates,” 2017.

[22] C. Sinck, “A Mass Optimization Study of the Lunar Zebro Chassis,” 2023.

[23] “falcon-users-guide,” 2025. [Online].

[24] M.-T. Tran, H.-A. Pham, V.-L. Nguyen and A.-T. Trinh, “Optimisation of stiffeners for maximum fundamental frequency of cross-ply laminated cylindrical panels using social group optimisation and smeared stiffener method,” *Thin-Walled Structures,* pp. 172-179, 2017.

[25] R. Sett, P. . P. Verekar and M. Zuber, “Comparative Study of Dimple Effect on Three-Dimensional Cambered Aircraft Wing,” *Journal of advance research in Fluid Mechanics and Thermal sciences,* p. 115–126, 2023.